ARTICLES
https://doi.org/10.1038/s41593-019-0514-0

nature neuroscience

Corrected: Author Correction

Noradrenergic signaling in the wakeful state inhibits microglial surveillance and synaptic plasticity in the mouse visual cortex

Rianne D. Stowell[1,2,7], Grayson O. Sipe[3,7], Ryan P. Dawes[1,2], Hanna N. Batchelor[1], Katheryn A. Lordy[1], Brendan S. Whitelaw[1,2], Mark B. Stoessel[1,2], Jean M. Bidlack[4], Edward Brown[5], Mriganka Sur[3] and Ania K. Majewska[1,6*]

Microglia are the brain's resident innate immune cells and also have a role in synaptic plasticity. Microglial processes continuously survey the brain parenchyma, interact with synaptic elements and maintain tissue homeostasis. However, the mechanisms that control surveillance and its role in synaptic plasticity are poorly understood. Microglial dynamics in vivo have been primarily studied in anesthetized animals. Here we report that microglial surveillance and injury response are reduced in awake mice as compared to anesthetized mice, suggesting that arousal state modulates microglial function. Pharmacologic stimulation of β_2-adrenergic receptors recapitulated these observations and disrupted experience-dependent plasticity, and these effects required the presence of β_2-adrenergic receptors in microglia. These results indicate that microglial roles in surveillance and synaptic plasticity in the mouse brain are modulated by noradrenergic tone fluctuations between arousal states and emphasize the need to understand the effect of disruptions of adrenergic signaling in neurodevelopment and neuropathology.

It is becoming increasingly clear that astrocytes and microglia are critical components of the 'quad-partite' synapse[1]. Microglia, the innate immune cells of the central nervous system (CNS), are exquisitely sensitive to changes in brain homeostasis and rapidly alter their morphology to respond to inflammatory signals. In the absence of injury or disease, microglial arbors are highly ramified with dynamic processes that continually extend and retract through the parenchyma[2,3]. Several recent in vivo imaging studies showed that these dynamics permit microglial interactions with neural elements in diverse regions of the CNS[4–7], allowing microglia to modulate synaptic remodeling and neural plasticity through the release of growth factors and enzymes or through physical synaptic contact[8–10]. Although several signaling pathways, such as fractalkine, complement and purinergic signaling, have been identified as mediating microglial function during neural circuit pruning, development and plasticity[8,10–13], other CNS signals, such as neurotransmitters, likely also play an important role and need to be considered[14].

Recent evidence suggests that glial physiology can be dramatically altered during wakeful states. For example, astrocytic calcium signaling increases in awake mice[15]. However, studies of microglia have been performed primarily in reduced preparations or in anesthetized animals, leaving open the possibility that microglial dynamics and the resulting interactions with neurons may be altered in awake brains. In addition, evidence suggests that extracellular space may increase under sedation[16], which could greatly affect microglial surveillance and thereby contribute to enhanced remodeling of synaptic structure[17] and increased activity-dependent plasticity[18]. Interestingly, in the non-injured brain, microglia have a high and selective expression of the β_2-adrenergic receptor (β_2-AR) relative to other CNS cell types[19,20], suggesting that they may have unique responses to norepinephrine (NE), which potently modulates plasticity, learning, attention to salient stimuli and sensory processing[17]. Furthermore, NE and β_2-ARs can affect the microglial inflammatory response[19], interleukin (IL)-1β production[20] and ATP-driven chemotaxis by inhibiting the $P2Y_{12}$ $G\alpha_i$ signaling pathway[21]. $P2Y_{12}$ is also critical for experience-dependent plasticity in the mouse adolescent visual system, and its loss impairs both the microglial response and synaptic plasticity itself[10]. Thus, NE could act through microglial β_2-ARs to modulate microglial behavior in the awake state and modulate $P2Y_{12}$-dependent microglial processes that contribute to activity-dependent synaptic rearrangement.

Here we demonstrate that microglia in the awake brain have smaller arbors and reduced parenchyma surveillance, and are less responsive to injury than those in anesthetized animals, suggesting that microglial functions in awake conditions are fundamentally different from what has previously been described under anesthesia. We then recapitulate most of these changes through pharmacologic stimulation or inhibition of microglial β_2-ARs. We demonstrate that microglial β_2-ARs and cortical NE release are necessary for the morphologic changes between awake and anesthetized states. Finally, we demonstrate that activation of microglial β_2-ARs impairs ocular dominance plasticity and microglial interactions with dendritic spines. Our work shows the importance of microglial β_2-AR signaling in regulating microglial surveillance of the brain as well as the participation of these cells in experience-dependent plasticity.

[1]Department of Neuroscience, University of Rochester Medical Center, Rochester, NY, USA. [2]Neuroscience Graduate Program, University of Rochester Medical Center, Rochester, NY, USA. [3]Picower Institute for Learning and Memory, Department of Brain and Cognitive Sciences, Massachusetts Institute of Technology, Cambridge, MA, USA. [4]Department of Pharmacology and Physiology, University of Rochester Medical Center, Rochester, NY, USA. [5]Department of Biomedical Engineering, University of Rochester, Rochester, NY, USA. [6]Center for Visual Science, University of Rochester Medical Center, Rochester, NY, USA. [7]These authors contributed equally: Rianne D. Stowell, Grayson O. Sipe. *e-mail: ania_majewska@urmc.rochester.edu

Results

Anesthesia increases microglial surveillance and injury response in the cortex parenchyma. Most studies of microglial dynamics in vivo were conducted in anesthetized animals or in ex vivo slice preparations[2,3,10,14]. However, anesthesia substantially alters numerous facets of brain physiology through diverse actions on multiple cell types. To determine whether microglial behavior is affected by anesthesia, we imaged microglial dynamics in the same adult animals when anesthetized and awake using the microglia-labeled CX3CR1^{GFP} transgenic mouse line (in which GFP is expressed under the control of the *Cx3cr1* promoter) and a chronic cranial window preparation. We found that microglia had more elaborate process arbors when mice were anesthetized with a commonly used fentanyl cocktail (also containing dexmedetomidine (DEX) and midazolam) as compared to when the animals were awake (Fig. 1a–d; area under the curve (AUC): paired *t*-test, $P<0.001$; maximum number of intersections: paired *t*-test, $P<0.001$). We next examined microglial process surveillance across 1 h to determine whether the decreased process ramification during wakefulness resulted in decreased parenchymal surveillance. We found a significant reduction in the total parenchymal area occupied by microglial processes in awake as compared to anesthetized states (Fig. 1e,f; paired *t*-test; $P<0.01$; Supplementary Videos 1 and 2). It is important to note that this definition of surveillance is based on a quantitative analysis and does not address qualitative changes in microglial surveillance capabilities.

Despite the animals being habituated to head restraint before imaging, it is possible that changes in microglial morphology and surveillance in awake animals are due to factors released as a result of increased stress. To test this possibility, we imaged microglia in animals that were exposed to restraint stress before anesthesia and found no difference in microglial motility, morphology or surveillance (Supplementary Fig. 1). We also determined that microglial morphology, surveillance and motility did not exhibit a circadian rhythmicity in anesthetized animals (Supplementary Fig. 2). On the basis of these findings, we concluded that anesthesia produces a more complex microglial morphology and higher process coverage of the brain parenchyma.

Given the significant effect of anesthesia on microglial surveillance and morphology, we next investigated whether these changes could affect targeted microglial responses to acute injury. We generated focal laser ablation injuries in the cortex of the same mice while they were either awake or anesthetized and quantified the injury response of microglia in the immediate surrounding tissue over 1 h (Fig. 1g and Supplementary Videos 3 and 4). We did not observe blood–brain barrier (BBB) disruption or monocyte infiltration during this period, suggesting that the GFP+ process responses were predominantly from surrounding microglia (Supplementary Fig. 3). We found that microglia had an increased response to focal tissue injury during anesthesia as measured by the magnitude of vectors generated by the movement of microglial processes toward the injury core (Fig. 1h–j; AUC: paired *t*-test, $P<0.05$; maximum response: paired *t*-test, $P=0.08$). The enhanced injury response and surveillance in anesthetized conditions suggest that wakefulness exerts a primarily inhibitory effect on microglial dynamics that is alleviated by anesthesia.

Norepinephrine release from the locus coeruleus inhibits microglial process dynamics. Anesthesia has varying effects on brain function depending on the methods and drug compositions used. Local field potential (LFP) recordings in the cortex showed that delta wave power was significantly lower in awake conditions (Fig. 1k,l), suggesting that the fentanyl cocktail puts the brain in a slow-wave–dominated state. To disambiguate the sedative effects from the analgesic effects of the fentanyl cocktail on microglia, we repeated our experiments using only DEX, which is a known sedative that reduces NE release from the locus coeruleus (LC) and has been used to approximate natural slow-wave sleep[21]. Treatment with DEX alone produced a robust increase in the size of microglial arbor (Fig. 2a–d; AUC: paired *t*-test, $P<0.05$; maximum number of intersections: paired *t*-test, $P<0.05$) and enhanced microglial surveillance (Fig. 2e,f; paired *t*-test, $P<0.05$; Supplementary Video 5). These effects are unlikely to be mediated by direct action of DEX on microglia, as microglial surveillance was not affected when DEX was applied to acute cortical slices (Supplementary Fig. 4). To examine the dynamics of DEX-elicited changes, we imaged microglia continuously during DEX administration and observed expansions in the arbors of the same microglia after DEX (Supplementary Fig. 5a–c). DEX-elicited morphologic changes were fairly rapid, occurring within ~15 min of intraperitoneal administration and were quickly reversible using atipamezole (Supplementary Fig. 5d–f). To explore the rapid alteration in microglial process dynamics with DEX, we used resonance two-photon imaging to capture microglial images with high temporal resolution. We found that in awake mice fine, transient filopodia rapidly extended and retracted from the main process arbor[22]. On the other hand, pseudopodia—the bulbous endings of microglial processes where extension and retraction of terminal processes occurs—were reduced (Supplementary Fig. 5g). DEX rapidly increased the ratio of pseudopodia formation (Supplementary Video 6) relative to filopodia formation (Fig. 2g,h; paired *t*-test, $P<0.001$), increasing the velocity and distance traveled of terminal microglial processes (Supplementary Fig. 5h–j) within ~10 min of administration. Thus, the effects of DEX on motility were complex, increasing the motility of terminal processes but decreasing overall motility due to the loss of motile filopodia (also observed under fentanyl anesthesia; Supplementary Fig. 6).

To dissect the microglial mechanisms responsible for our observations, we considered signaling pathways in microglia that could affect microglial process stabilization during wakeful states. Although $P2Y_{12}$ and CX3CR1 did not appear to mediate these effects (Supplementary Fig. 7), NE itself is a powerful mediator of wakefulness with decreased concentrations in the cortex during anesthesia[19,23]. Additionally, the sedative effects of DEX are thought to be mediated by suppressing LC activity via auto-receptor inhibition, decreasing cortical NE release. To test whether endogenous NE release is necessary for the observed effects of DEX, we used the LC-selective neurotoxin *N*-(2-chloroethyl)-*N*-ethyl-2-bromobenzylamine (DSP4; 2 d before imaging; Supplementary Fig. 8) to ablate LC axons to the cortex and compared microglial morphology in awake animals before and after DEX treatment without LC axons. We found that DSP4 treatment prevented the increased microglial arborization (Fig. 2i–k; paired *t*-test, $P>0.05$) and reversed the increase in surveillance (Fig. 2l; paired *t*-test, $P<0.05$) previously observed with DEX treatment. We then investigated whether optogenetic stimulation of axons locally under DEX treatment is sufficient to alter microglial process dynamics by generating a CX3CR1^{GFP}/TH-Cre mouse (expressing Cre recombinade from the *Th* promoter) and bilaterally injecting virus encoding *loxP*-flanked (floxed) ChR2 in the LC. In DEX-treated animals, optogenetic activation of LC axons in the cortex resulted in decreased process surveillance (Fig. 2m,n; two-way repeated measures (RM) ANOVA, $P<0.05$). These data suggest that NE release from the LC during wakeful states reduces microglial process morphology and parenchymal surveillance.

β_2-AR agonism in anesthetized mice decreases microglial process ramification. NE exerts diverse effects on multiple cell types through a family of G-protein-coupled receptors (GPCRs). Although it is possible that NE exerts its effects on microglia through indirect pathways involving other cell types, we focused on the direct effect on β_2-ARs because microglia are known to express β_2-ARs at higher levels than other CNS cell types in the healthy

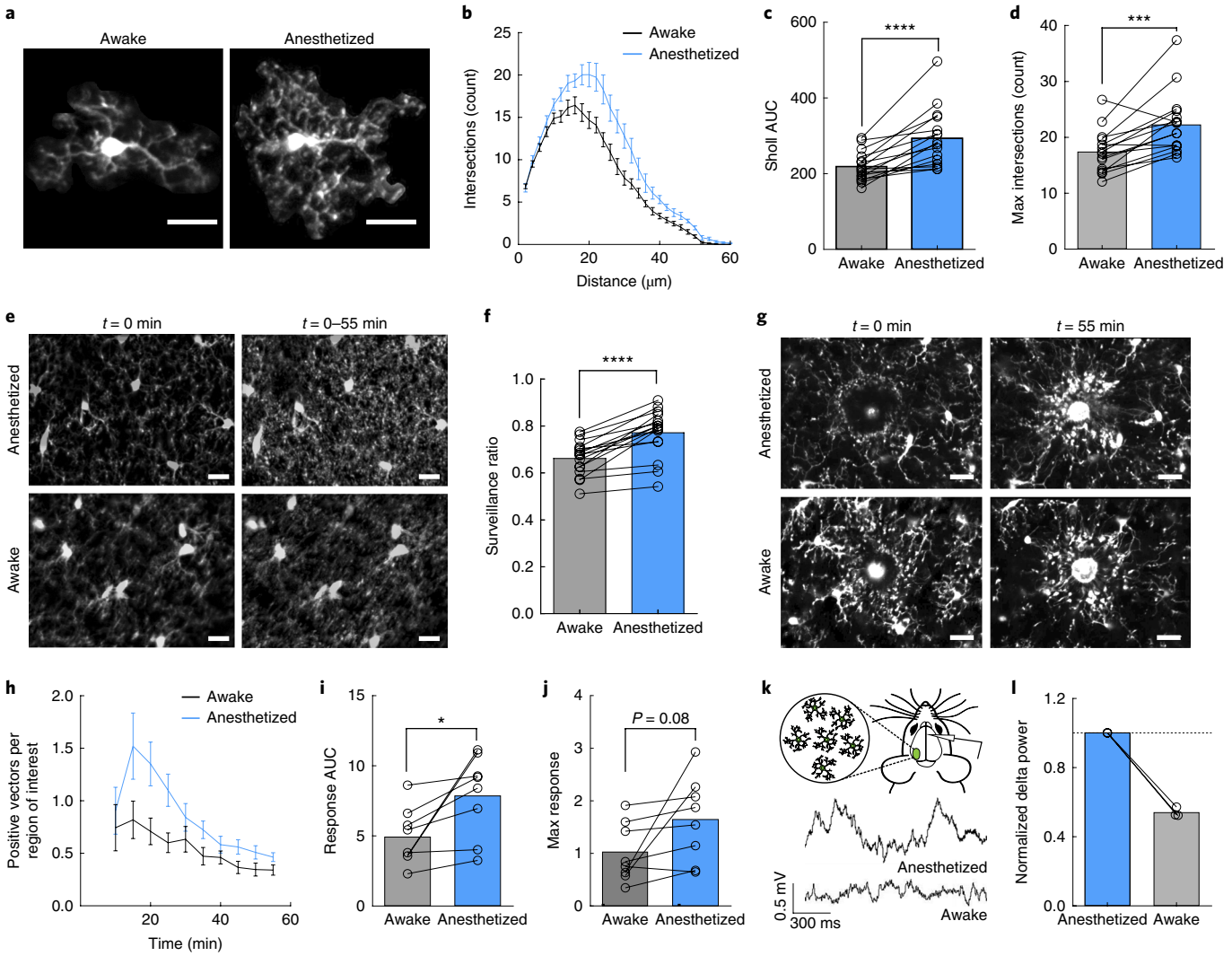

Fig. 1 | Anesthesia enhances microglial surveillance of the parenchyma. a, Individual microglia from awake and anesthetized mice. **b**, Sholl profiles of microglia in awake (black) and anesthetized (blue) mice; note the reduced arborization in awake mice ($n = 16$ mice, 3–5 microglia per mouse). **c**, Microglia have a greater AUC in anesthetized versus awake mice ($n = 16$ mice; two-sided paired t-test, $P = 8.9 \times 10^{-5}$, $t(15) = 5.30$). **d**, Microglia have more maximum intersections in anesthetized mice ($n = 16$ mice; two-sided paired t-test, $P = 0.00051$, $t(15) = 4.40$). **e**, Two-dimensional maximum projection of microglial processes at the first time point ($t = 0$ min) and over 1 h of imaging ($t = 0$–55 min) to quantify process surveillance. **f**, Microglia in anesthetized animals cover more of the CNS parenchyma ($n = 16$ mice; two-sided paired t-test, $P = 8.2 \times 10^{-6}$, $t(15) = 6.62$). **g**, Microglia in an awake or anesthetized mouse surrounding a focal laser ablation injury at $t = 0$ and $t = 55$ min after ablation. **h**, Graph of microglial process recruitment from 10 min after injury to 55 min after injury (velocity magnitude of responding vectors/total region of interest pixels; $n = 8$ mice). **i**, Response AUC of microglial process recruitment from 10–55 min after injury ($n = 8$ mice; two-sided paired t-test, $P = 0.025$, $t(7) = 2.84$). **j**, Microglia trend toward a greater maximum magnitude of injury response in anesthetized conditions ($n = 8$ mice; two-sided paired t-test, $P = 0.077$, $t(7) = 2.08$). **k**, Example LFP traces in anesthetized and awake conditions. **l**, Normalized delta power from LFP recordings demonstrating decreased delta power (~54%) in the awake state relative to the anesthetized state ($n = 3$ mice). Scale bars, 20 μm. Graphs show mean ± s.e.m.; $^*P < 0.05$, $^{**}P < 0.01$, $^{***}P < 0.005$, $^{****}P < 0.0001$. Points represent individual animals. See Supplementary Table 1 for the numbers of females and males used in these experiments.

brain[20]. In addition, previous in vitro work demonstrated that microglial β_2-AR signaling can inhibit chemotaxis toward ATP[24]. To test whether β_2-AR signaling alters microglial dynamics in vivo, we systemically applied the BBB-permeant β_2-AR selective agonist clenbuterol in fentanyl-anesthetized mice. To account for indirect clenbuterol effects through the periphery, mice were pre-dosed with the BBB-impermeant, non-selective β-AR antagonist nadolol at least 1 h before clenbuterol dosing. Clenbuterol treatment caused a significant and sustained retraction of microglial processes, resulting in microglia that resembled those seen in awake mice (Fig. 3a). Microglial pseudopodia retracted within the first 30 min of imaging (Fig. 3b; two-way ANOVA, $P < 0.001$), and new pseudopodia were less likely to be formed (Supplementary Fig. 9a). In addition, we also observed a persistent decrease in microglial motility as compared to saline-treated mice (Supplementary Fig. 9b; two-way ANOVA, $P < 0.01$), despite a return to baseline pseudopodia dynamics in the second half-hour of imaging. To further validate that the effects of β_2-AR agonism were a direct effect on microglia and not due to peripheral activation of β_2-ARs, we directly applied a selective β_2-AR agonist, terbutaline, through an acute craniotomy and replicated our effects from the intraperitoneal clenbuterol administration (Supplementary Fig. 10 and Supplementary Video 7).

To further quantify the sustained effect of clenbuterol on microglia in fentanyl-anesthetized mice, we traced individual microglia

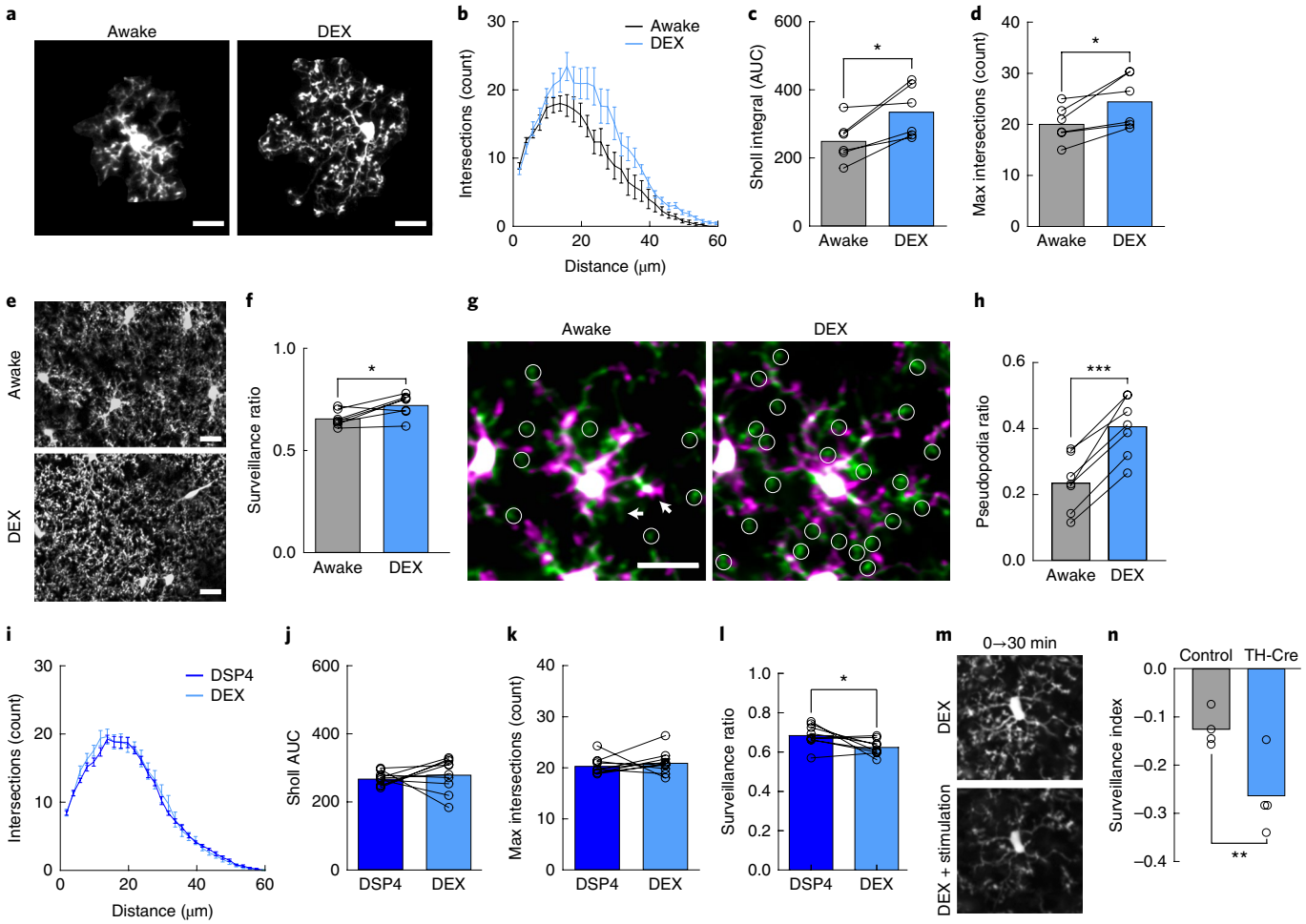

Fig. 2 | Microglial surveillance is enhanced by DEX. a, Example microglia in awake or DEX-anesthetized mice. **b**, Sholl profiles of microglia in awake (black) and DEX-treated (blue) mice; note the increased ramification of the microglial arbor with DEX ($n=7$ mice, 3–5 microglia per mouse). **c**,**d** Microglia in DEX-treated mice have a greater AUC than those in awake mice ($n=7$ mice, two-sided paired t-test, $P=0.015$, $t(5)=3.63$) (**c**) and a greater number of maximum process intersections ($n=7$ mice; two-sided paired t-test, $P=0.024$, $t(6)=3.20$) (**d**). **e**, Two-dimensional maximum projection of microglial processes over 1 h of imaging to quantify process surveillance. **f**, Microglia in DEX-treated mice survey a greater portion of the CNS parenchyma ($n=7$ mice; two-sided paired t-test, $P=0.020$, $t(5)=3.13$). **g**, Overlays images taken at of two time points 10 min apart in awake and DEX-treated mice. Notice the increase in the extension of pseudopodia (circles) after DEX. Arrows indicate filopodial extension (green) and retraction (magenta) in the awake state. **h**, Quantification of the pseudopodia ratio showing a higher proportion of pseudopodia in DEX-treated animals ($n=7$ mice; two-sided paired t-test, $P=0.00010$, $t(6)=9.01$). **i**, Sholl profiles of DSP4-treated animals when awake (dark blue) and under DEX (light blue; $n=10$ mice, 3–5 microglia per mouse). **j**, Sholl AUC showing no difference between awake and DEX-treated miceunder DSP4 treatment ($n=10$ mice; two-sided paired t-test, EMP21 = 0.55, $t(9)=0.63$). **k**, Awake and DEX-treated mice similarly show no significant difference in the maximum process intersections ($n=10$ mice; two-sided paired t-test, $P=0.50$, $t(9)=0.69$). **l**, DSP4-treated mice have a decreased surveillance ratio with DEX treatment ($n=9$ mice; two-sided paired t-test, $P=0.038$, $t(8)=2.48$). **m**, Two-dimensional maximum projection of microglial processes over 30 min in DEX-treated mice before and after optogenetic stimulation of LC axons in the cortex. **n**, Stimulation decreased the microglial surveillance index (laser-stimulated surveillance – baseline surveillance/baseline surveillance) to a larger degree in CX3CR1^{GFP}/TH-Cre mice than in light-control CX3CR1^{GFP} mice (mice had a single copy of the transgenes; $n=4$ mice; two-sided t-test, $P=0.022$, $t(6)=3.08$). Scale bars, 20 μm. Graphs show mean ± s.e.m.; $^{*}P<0.05$, $^{**}P<0.01$, $^{***}P<0.005$. Points represent individual animals. See Supplementary Table 1 for the numbers of females and males used in these experiments.

and used Sholl analysis to assay the complexity of the arbor. We found that microglia treated with clenbuterol 2 h before imaging had significantly reduced arbor complexity (Fig. 3c–f; AUC: one-way ANOVA, $P<0.001$; maximum number of intersections: one-way ANOVA, $P<0.001$). Beginning 3 h after administration, clenbuterol-treated animals exhibited a significant decrease in microglial process coverage of the parenchyma over 1 h of imaging (Fig. 3g,h; one-way ANOVA; $P<0.001$). To assess whether the observed effects of acute clenbuterol administration produced sustained changes in microglial dynamics, we examined microglial motility 3 h after clenbuterol injection and found that it was not significantly reduced (Supplementary Fig. 11 and Supplementary Videos 8–10).

To further dissect the effects of β_2-AR signaling on microglial dynamics, we asked whether reducing microglial β_2-AR signaling affected microglial dynamics under fentanyl anesthesia. DSP4 injection 48 h before imaging reduced microglial surveillance (Fig. 3h; two-way ANOVA, $P<0.05$) and decreased microglial motility (Supplementary Fig. 11 and Supplementary Video 11), whereas administering the β_2-AR antagonist ICI-118,551 (at the time of imaging) to selectively block β_2-AR signaling had no effect (Fig. 3h, Supplementary Fig. 11 and Supplementary Video 12).

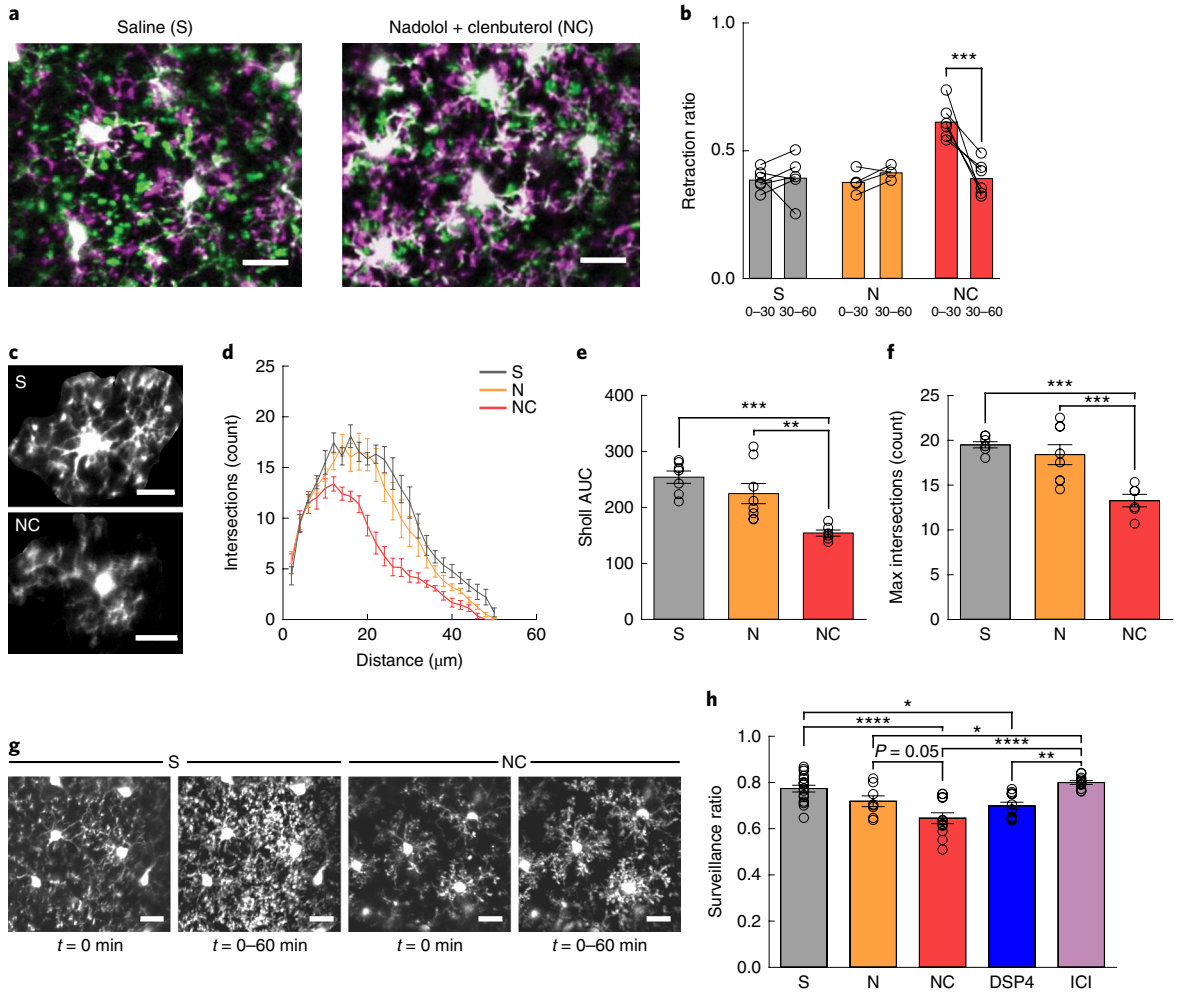

Fig. 3 | β_2-AR signaling reduces microglial dynamics in adolescent mice. Anesthetized mice were imaged through a thin-skull preparation. **a**, Overlay of microglia at $t = 0$ min (magenta) and $t = 30$ min (green) in mice treated with saline (S) or with nadolol and clenbuterol (NC); note the increased retraction of processes (magenta) in mice treated with nadolol and clenbuterol. **b**, Microglia in mice treated with nadolol and clenbuterol but not with saline or nadolol alone (N) have a rapid transient increase in the retraction ratio (retracted pseudopodia/total pseudopodia) from 0–30 min ($n = 6$ (S), 5 (N) and 6 (NC) mice; two-way RM-ANOVA: significant main effects of treatment ($P = 0.00084$, $F(2,13) = 12.82$), time ($P = 0.0018$, $F(1,13) = 15.27$) and interaction ($P = 0.0026$, $F(2,13) = 9.72$); Holm–Sidak multiple comparisons: S versus NC, $P = 0.00011$). **c**, Example microglia from mice treated with saline or with nadolol and clenbuterol. **d**, Sholl profiles of mice treated with saline, nadolol alone, or nadolol and clenbuterol; note the reduction in microglial arborization in mice treated with nadolol and clenbuterol ($n = 7$ (S), 8 (N) and 6 (NC) mice, 3–5 microglia per animal). **e**, Treatment with nadolol and clenbuterol reduces Sholl AUC ($n = 7$ (S), 8 (N) and 6 (NC) mice; one-way ANOVA: $P = 0.00040$, $F(2,18) = 12.45$; Holm–Sidak multiple comparisons: S versus NC, $P = 0.00036$; N versus NC, $P = 0.0045$). **f**, The maximum number of Sholl intersections is reduced in microglia from mice treated with nadolol and clenbuterol ($n = 7$ (S), 8 (N) and 6 (NC) mice; one-way ANOVA: $P = 0.00019$, $F(2,18) = 14.31$; Holm–Sidak multiple comparisons: S versus NC, $P = 0.00025$; N versus NC, $P = 0.00091$). **g**, Initial ramification ($t = 0$ min) and two-dimensional maximum projections ($t = 0$–60 min) of microglial process surveillance in mice treated with saline or with nadolol and clenbuterol; note the decreased surveillance in the mice treated with nadolol and clenbuterol. **h**, Microglia in mice treated with nadolol and clenbuterol or with DSP4 survey less of the parenchyma ($n = 16$ (S), 8 (N), 12 (NC), 12 (DSP4) and 11 (ICI-118,551, ICI) mice; one-way ANOVA: $P = 2.6 \times 10^{-7}$, $F(4,55) = 12.51$; Holm–Sidak multiple comparisons: S versus NC, $P = 6.6 \times 10^{-6}$; S versus DSP4, $P = 0.013$; N versus ICI, $P = 0.034$; NC versus ICI, $P = 1.1 \times 10^{-6}$; DSP4 versus ICI, $P = 0.0015$). Scale bars, 20 μm. Graphs show mean ± s.e.m; $^*P < 0.05$, $^{**}P < 0.01$, $^{***}P < 0.005$, $^{****}P < 0.0001$). Points represent individual animals. See Supplementary Table 1 for the numbers of females and males used in these experiments.

β_2-AR antagonism in awake mice increases microglial process ramification. Because β_2-AR agonism decreased microglial ramification and surveillance in anesthetized animals, we investigated whether similar effects occur without anesthesia. Awake mice imaged through cranial windows were treated with either clenbuterol or ICI-118,551 to selectively stimulate and block β_2-AR signaling, respectively (Fig. 4a). Sholl analysis revealed that clenbuterol had no effect on microglial ramification in awake mice (Fig. 4a–c,e; AUC: paired t-test, not significant (NS); maximum number of intersections: paired t-test, NS), whereas ICI-118,551 increased ramification (Fig. 4a,b,d,f; AUC: paired t-test, $P < 0.001$; maximum response; paired t-test, $P < 0.001$). We found that clenbuterol significantly reduced microglial surveillance of the parenchyma, despite the lack of effect on microglial arborization (Fig. 4g,h; paired t-test, $P < 0.01$). We also found that microglia from ICI-118,551-treated mice showed enhanced surveillance of the parenchyma (Fig. 4g,i; paired t-test, $P < 0.05$). In addition, we examined motility and found that clenbuterol significantly reduced microglial motility (Supplementary Fig. 12a) whereas ICI-118,551 significantly increased microglial motility in awake mice

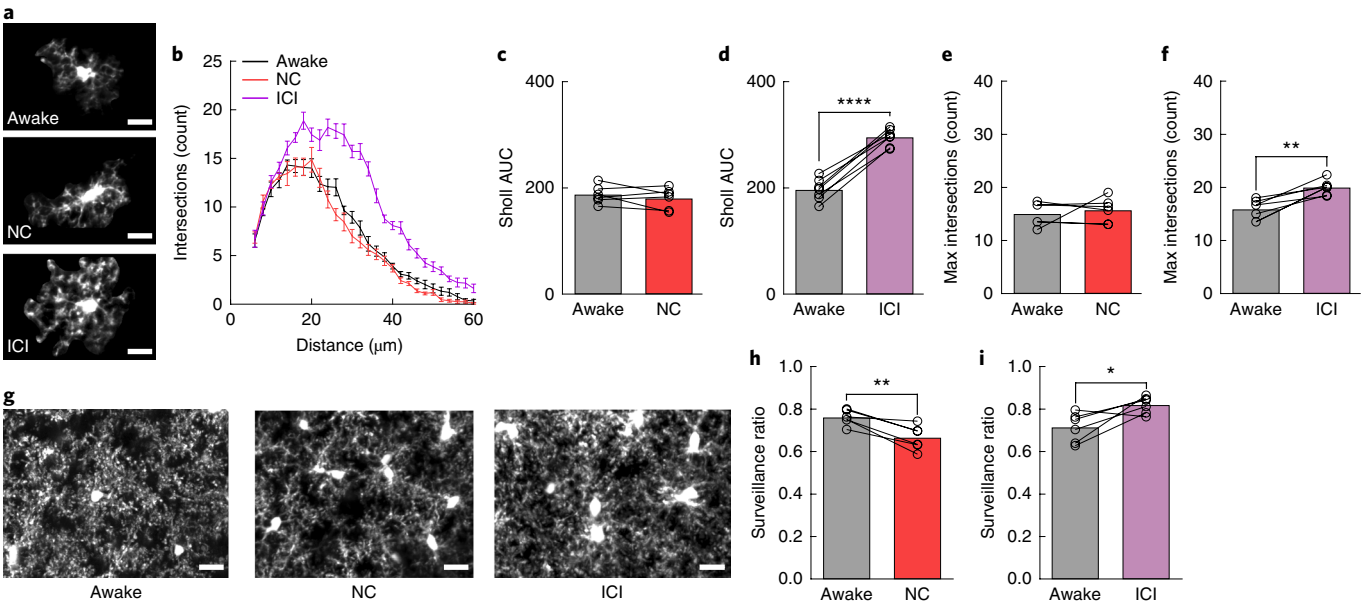

Fig. 4 | Inhibition of β_2-ARs in awake mice recapitulates the effects of anesthesia by enhancing microglial arborization and surveillance. a, Microglia from untreated awake mice and mice treated with nadolol and clenbuterol or with ICI-118,551. **b**, Sholl profiles of microglia in awake mice before (gray) and after treatment with nadolol and clenbuterol (red) or ICI-118,551 (purple) ($n = 6$ (NC) and 7 (ICI) mice, 3–5 microglia per animal); note the increase in microglial process arborization with ICI-118,551 treatment. **c**, The Sholl AUC of awake mice given nadolol and clenbuterol is not altered ($n = 6$ mice; two-sided paired t-test, $P = 0.36$, $t(5) = 1.00$). **d**, ICI-118,551 treatment increases the Sholl AUC in awake mice ($n = 7$ mice; two-sided paired t-test, $P = 5.8 \times 10^{-6}$, $t(6) = 14.89$). **e**, The maximum number of Sholl intersections is not altered with nadolol and clenbuterol in awake mice ($n = 6$ mice; two-sided paired t-test, $P = 0.60$, $t(5) = 0.56$). **f**, The maximum number of Sholl intersections is increased by ICI-118,551 in awake mice ($n = 7$ mice; paired t-test, $P = 0.0019$, $t(6) = 5.24$). **g**, Two-dimensional maximum projections of microglial process surveillance from 0–60 min; note the decreased surveillance after treatment with nadolol and clenbuterol and the increased surveillance after treatment with ICI-118,551. **h**, Microglia in awake mice treated with nadolol and clenbuterol survey less of the parenchyma ($n = 6$ mice; two-sided paired t-test, $P = 0.0045$, $t(5) = 4.89$). **i**, Microglia in ICI-118,551-treated awake mice have increased surveillance of the parenchyma ($n = 6$ mice; two-sided paired t-test, $P = 0.029$, $t(5) = 3.03$). Scale bars, 20 μm. Graphs show mean ± s.e.m.; $^*P < 0.05$, $^{**}P < 0.01$, $^{***}P < 0.005$, $^{****}P < 0.0001$). Points represent individual animals. See Supplementary Table 1 for the numbers of females and males used in these experiments.

(Supplementary Fig. 12b and Supplementary Video 13). Combined with our previous data in awake versus anesthetized mice, these data suggest that, during wakeful conditions, microglial ramification and process motility are inhibited by endogenous NE, and that relieving this inhibition via β_2-AR antagonism induces an increase in process ramification and surveillance, recapitulating the effects of anesthesia.

β_2-AR signaling affects microglial response to focal tissue injury. Previous work showed that both NE and β-AR stimulation block microglial process chemotaxis to ATP in vitro[24], suggesting that β-AR signaling may attenuate microglial responses to injury-induced ATP release. To determine whether this is also true in vivo, we created a focal laser tissue injury in adolescent fentanyl-anesthetized mice and observed reduced microglial process recruitment to the lesion core in clenbuterol-treated mice (Fig. 5a,b and Supplementary Videos 14 and15). We observed that peak response and overall microglial response to the injury were significantly reduced in clenbuterol-treated mice (Fig. 5c–e; one-way ANOVA, $P < 0.0001$). Furthermore, there was a trend toward an increased response in nadolol- or ICI–118,551-treated mice (Fig. 5c–e; one-way ANOVA, $P = 0.12$). These data suggest that microglial β_2-AR signaling attenuates not only baseline surveillance but also the response to changes in CNS homeostasis during acute injury.

Noradrenergic signaling and β_2-AR stimulation impair critical period ocular dominance plasticity. After observing the robust effects of noradrenergic and β_2-AR signaling on microglia, we investigated whether this signaling pathway mediates microglial roles in synaptic plasticity. Previously published work from our laboratory showed that microglial processes interact with neural elements in vivo[4,7,10] and that these interactions can be modulated by visual experience[4]. We also showed that, during the mouse adolescent visual critical period, perturbation of microglial purinergic signaling through $P2Y_{12}$ impairs ocular dominance plasticity (ODP)[10]. Given the antagonistic effect of β_2-ARs on $P2Y_{12}$ signaling[24], we hypothesized that microglial β_2-AR signaling might impair ODP during the peak of the mouse visual critical period (at approximately postnatal day (P) 25 through P32; refs. [25,26]) when our experiments have demonstrated altered microglial phenotypes (Figs. 1–4). Selectively activating β_2-ARs chronically with clenbuterol effectively blocked ODP, as indicated by a lack of ocular dominance shift of neuronal responses after 4 d of monocular deprivation (Fig. 6a–c; two-way ANOVA, $P < 0.001$). Both saline-treated mice and mice treated only with nadolol showed normal ocular dominance shifts, indicating intact ODP (Fig. 6b,c). In addition, cortical NE depletion with DSP4 treatment impaired ODP, confirming previous work demonstrating that NE has important roles in ODP (Fig. 6c)[27]. However, this effect appeared to be independent of β_2-AR signaling, as chronic blockade of β_2-ARs with ICI-118,551 did not affect ODP (Supplementary Fig. 13). Thus, sustained stimulation of β_2-AR signaling interferes with the plastic processes that mediate ODP, but NE signaling through other signaling pathways is necessary for ODP[28]. β_2-AR stimulation may impair ODP by modulating microglial surveillance and limiting microglial interactions with synapses. To examine this possibility, we used $CX3CR1^{GFP}/THY1^{YFP}$ mice (expressing yellow fluorescent protein (YFP) from the *Thy1* promoter) to simultaneously image microglia and dendrites in mice in the visual critical

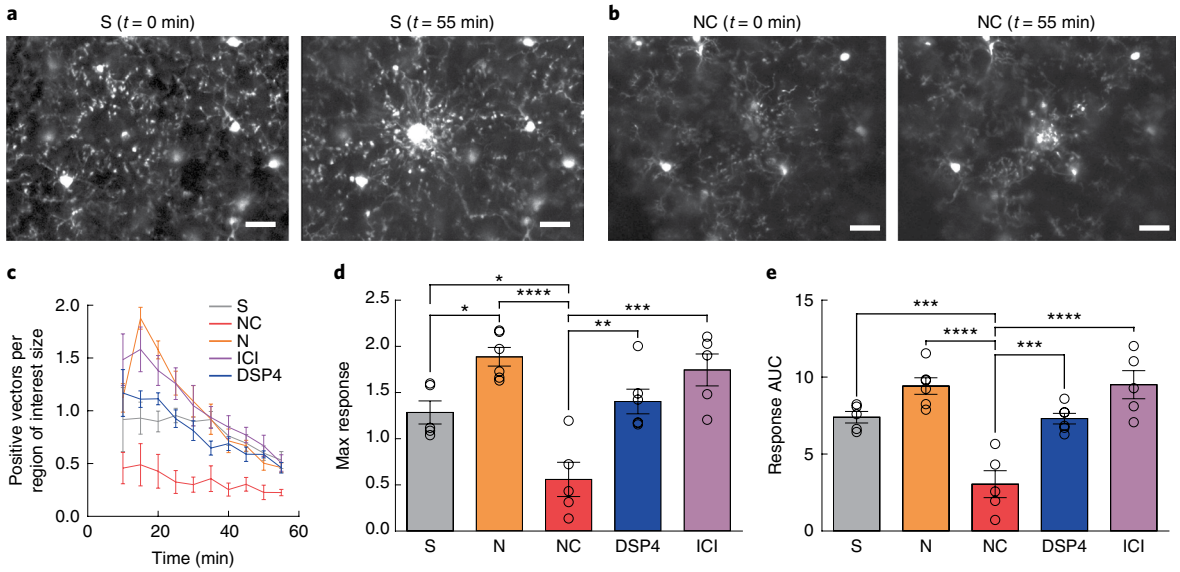

Fig. 5 | β_2-AR activation inhibits microglial process response to focal tissue injury. a, Example microglial response to focal laser ablation in a saline-treated mouse at $t = 0$ min and $t = 55$ min after ablation. **b**, Example microglial response to laser ablation in a mouse treated with nadolol and clenbuterol at $t = 0$ min and $t = 55$ min after ablation. **c**, Microglial process response vectors from 10–55 min after ablation ($n = 5$ (S), 7 (N), 5 (NC), 6 (DSP4) and 6 (ICI) mice). **d**, Microglia in mice treated with nadolol and clenbuterol have a reduced maximum response to focal tissue injury ($n = 5$ (S), 7 (N), 5 (NC), 6 (DSP4) and 6 (ICI) mice; one-way ANOVA: $P = 1.7 \times 10^{-5}$, $F(4,26) = 12.69$; Holm–Sidak multiple comparisons: S versus NC, $P = 0.016$; S versus N, $P = 0.039$; N versus NC, $P = 1.3 \times 10^{-5}$; NC versus DSP4, $P = 0.0031$; NC versus ICI, $P = 0.00010$). **e**, Microglia in mice treated with nadolol and clenbuterol have a decreased response AUC 10–55 min after ablation ($n = 5$ (S), 7 (N), 5 (NC), 6 (DSP4) and 6 (ICI) mice; one-way ANOVA: $P = 2.1 \times 10^{-6}$, $F(4,26) = 16.65$; Holm–Sidak multiple comparisons: S versus NC, $P = 0.00073$; N versus NC, $P = 3.1 \times 10^{-6;}$ NC versus DSP4, $P = 0.00061$; NC versus ICI, $P = 4.5 \times 10^{-6}$). Scale bars, 20 µm. Graphs show mean ± s.e.m.; $^*P < 0.05$, $^{**}P < 0.01$, $^{***}P < 0.005$, $^{****}P < 0.0001$). Points represent individual animals. See Supplementary Table 1 for the numbers of females and males used in these experiments.

period. We found that β_2-AR stimulation, but not depletion of NE, significantly reduced microglial contacts with dendritic spines (Fig. 6d,e). This suggests that the effects of β_2-AR stimulation on ODP may arise, in part, from abnormal microglial–dendritic spine interactions, whereas depleting NE likely affects plasticity through other cell types.

Microglial β_2-AR activation impairs ocular dominance plasticity. Despite the known roles of microglia in ODP and high microglial β_2-AR expression, it is possible that pharmacologic β_2-AR stimulation impairs ODP through non-microglial pathways. To determine whether the observed results were specifically mediated through β_2-AR signaling in microglia, we crossed a CX3CR1-Cre^{ERT} mouse line (expressing Cre from the *Cx3cr1* promoter)[9] to β_2-AR-flox mice (in which both alleles of the *Adrb2* gene are *loxP*-flanked)[29] to selectively ablate β_2-ARs in microglia (Fig. 7a). Mice were dosed with tamoxifen from approximately P2–P4 (ref. [9]) to ensure that β_2-ARs were selectively ablated from microglia in adolescent mice. Microglia were isolated from tamoxifen-treated animals, and successful gene excision of β_2-AR was confirmed by PCR (Supplementary Fig. 14). To test whether the effects of β_2-AR stimulation on microglial dynamics were dependent on microglial β_2-AR expression, we labeled microglia by crossing these mice with the Ai9 reporter line (expressing a tdTomato construct inserted into the *(ROSA)26Sor* locus with a *loxP*-flanked STOP cassette preventing expression in the absence of Cre recombinase). Clenbuterol no longer induced retraction of the microglial arbor in tamoxifen-treated CX3CR1-Cre^{ERT}(heterozygous, het)/β_2-AR-flox/Ai9 mice, whereas the response was intact in control, tamoxifen-treated CX3CR1-Cre^{ERT}(het)/Ai9 mice (Fig. 7b,c; two-way ANOVA, $P < 0.001$), further indicating that microglial β_2-ARs are essential regulators of microglial responses to NE (Fig. 7d–f and h–j). We then repeated ODP experiments with tamoxifen-treated CX3CR1-Cre^{ERT}(het) controls and CX3CR1-Cre^{ERT}(het)/β_2-AR-flox mice (Fig. 7g,k). Control mice showed the same effects of pharmacologic manipulation as C57BL/6J mice (Fig. 7g; two-way ANOVA, $P < 0.001$) CX3CR1-Cre^{ERT}(het)/β_2-AR-flox mice lacking microglial β_2-ARs exhibited normal ODP, suggesting that microglial β_2-ARs are not necessary for ODP. We found that ablating β_2-ARs in microglia, however, rescued ODP during chronic clenbuterol administration (Fig. 7k; two-way ANOVA, NS (interaction)), suggesting that aberrant activity of microglial β_2-ARs interferes with normal plasticity. DSP4 treatment still blocked ODP in the CX3CR1-Cre^{ERT}(het)/β_2-AR-flox mice (Fig. 7k; two-way ANOVA, Holm–Sidak multiple comparisons test, $P < 0.05$). Our results demonstrate that microglial β_2-ARs are capable of blocking ODP, whereas cortical NE depletion likely blocks ODP through non-microglial mechanisms.

Discussion

We report that the microglial β_2-AR is a key receptor in regulating basal microglial surveillance and injury response in the visual cortex of awake mice and that chronic pharmacologic stimulation of this receptor during the mouse adolescent visual critical period impairs cortical experience-dependent plasticity. In wakeful conditions, microglial process arbors are small and highly motile, dominated mostly by filopodial protrusions. Anesthesia rapidly increases microglial arborization and pseudopodia extension, allowing microglial processes to survey a larger area of the cortex and respond more rapidly to a focal injury. Administration of the β_2-AR agonist clenbuterol in anesthetized mice results in microglial characteristics that resemble those of the awake state, whereas the β_2-AR antagonist ICI-118,551 generates microglial phenotypes that resemble those of anesthetized conditions in awake mice. Furthermore, ablation of β_2-ARs in microglia eliminates morphologic changes between awake and anesthetized states, suggesting that signaling through this microglial receptor regulates microglial

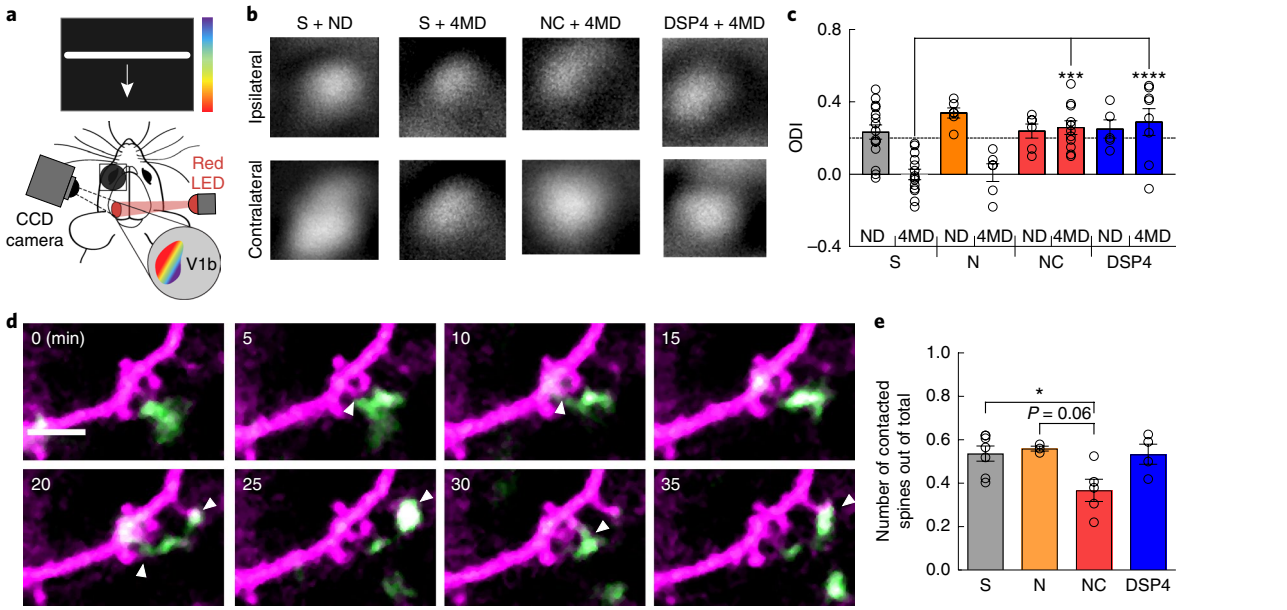

Fig. 6 | Chronic microglial β_2-AR activation impairs adolescent ODP. a, Schematic of the intrinsic optical signal imaging. **b**, Representative amplitude maps from stimulation of the ipsilateral (top) and contralateral (bottom) eyes for mice treated with saline, nadolol and clenbuterol, or DSP4. Non-deprived (ND) maps are shown for saline treatment. All other maps are after 4 d of monocular deprivation (4MD); these maps are representative of the presented findings. **c**, Quantification of the ocular dominance index (ODI) demonstrates ocular dominance shifts with saline and nadolol treatment but no shifts for treatment with nadolol and clenbuterol or DSP4 ($n = 15$ (S + ND), 14 (S + 4MD), 6 (N + ND), 6 (N + 4MD), 6 (NC + ND), 11 (NC + 4MD), 6 (DSP4 + ND) and 8 (DSP4 + 4MD) mice; two-way ANOVA: main effects of MD ($P = 0.00033$, $F(1,76) = 14.15$), treatment ($P = 0.0025$, $F(4,76) = 4.51$) and interaction ($P = 0.00035$, $F(4,76) = 5.89$); Holm–Sidak multiple comparisons: S + 4MD versus NC + 4MD, $P = 0.00014$; S + 4MD versus DSP4 + 4MD, $P = 1.0 \times 10^{-5}$). **d**, Example imaging of a single dendrite (magenta) and microglial process (green) across 35 min showing numerous putative microglial–dendritic spine interactions (white arrowheads). **e**, Treatment with nadolol and clenbuterol reduces the proportion of dendritic spines contacted by microglial processes over 1 h ($n = 7$ (S), 3 (N), 5 (NC) and 4 (DSP4) mice; one-way ANOVA: $P = 0.022$, $F(3,15) = 4.35$; Holm–Sidak multiple comparisons: S versus NC, $P = 0.041$; N versus NC, $P = 0.061$). Scale bar, 5 µm. Graphs show mean ± s.e.m.; $^*P < 0.05$, $^{**}P < 0.01$, $^{***}P < 0.005$. Points represent individual animals. See Supplementary Table 1 for the numbers of females and males used in these experiments.

function during wakefulness. Our findings indicate that there are robust differences in microglial basal dynamics between awake and anesthetic states and that these changes are driven by noradrenergic β_2-AR signaling in microglia (Supplementary Fig. 15).

Endogenous norepinephrine is a potent modulator of microglial function. NE is a potent neuromodulator that regulates brain function and elicits transitions between internal states such as wakefulness, arousal and stress. NE has many targets throughout the nervous system and can coordinate synchronized changes in multiple cell types through tonic signaling and phasic firing to salient or noxious stimuli[19]. Astrocytic function, for instance, is highly dependent on brain state with different roles during sleep, when NE is low, and wakefulness or stress, when NE is high[23]. Here we provide evidence that microglia, like astrocytes, may differ robustly between the awake and anesthetized state. Although we could not quantify microglial dynamics in sleeping animals, because mice have very short sleep cycles[23,30], our experiments with DEX suggest that microglia in mice may also show enhanced surveillance and injury responses during sleep. DEX is thought to hyperpolarize LC neurons and inhibit NE release throughout the brain[21], leading to brain activity that resembles the more prolonged slow-wave sleep in humans[30]. The idea that microglia behave differently in the awake versus sleeping brain merits further investigation, as many diseases are linked to changes in sleep patterns, and the quality of sleep can in turn greatly affect disease progression[31].

Noradrenergic inhibition of microglial dynamics impairs synaptic plasticity, suggesting that brain state, through noradrenergic signaling, modulates microglia–synapse interactions[4]. Simulating a chronic awake state through pharmacologic targeting of microglial β_2-ARs prevents ODP, further suggesting that microglia require decreased noradrenergic signaling to fulfill essential roles in neural plasticity. This implies that, in physiological conditions, NE may be exerting an important inhibitory function on microglia, perhaps preventing inappropriate or excessive microglia–neuron interactions. Our findings also suggest that increased noradrenergic signaling due to sleep deprivation or genetic conditions altering β_2-AR signaling may result in aberrant microglial participation in plasticity processes. In the awake state, tonic NE release decreases neural variability in firing rates and is thought to enhance the signal-to-noise ratio in the visual cortex[32]. NE bulk release from varicosities could enhance neural tuning while simultaneously inhibiting microglia–neuron interactions through selective activation of β_2-ARs. Previous work demonstrated that sleep is necessary for plasticity, as well as specifically for ODP[33], and, while many signals are regulated by sleep, microglial β_2-AR signaling may be an additional target. It is also important to note that microglial $P2Y_{12}$ is necessary for ODP, and both genetic and pharmacologic inhibition result in the loss of plasticity[10]. Thus, it is likely that interactions between β_2-AR and $P2Y_{12}$ signaling in microglia regulate microglial roles at synapses. The effects of NE on microglia and plasticity may also be mediated by NE signaling in other cell types. In our study, depletion of NE with the neurotoxin DSP4 blocked ODP and affected microglial motility; however, ablation of microglial β_2-ARs failed to rescue plasticity in DSP4-treated mice. This suggests that loss of NE in this model signals through a different receptor or cell type to alter microglial dynamics and plasticity. Interestingly, astrocytes have robust expression levels of α_1-, α_2- and β_1-ARs, which contribute to astrocytic metabolic coupling and K^+ clearing during neural activity[19]. The diverse effects of NE on astrocytic function

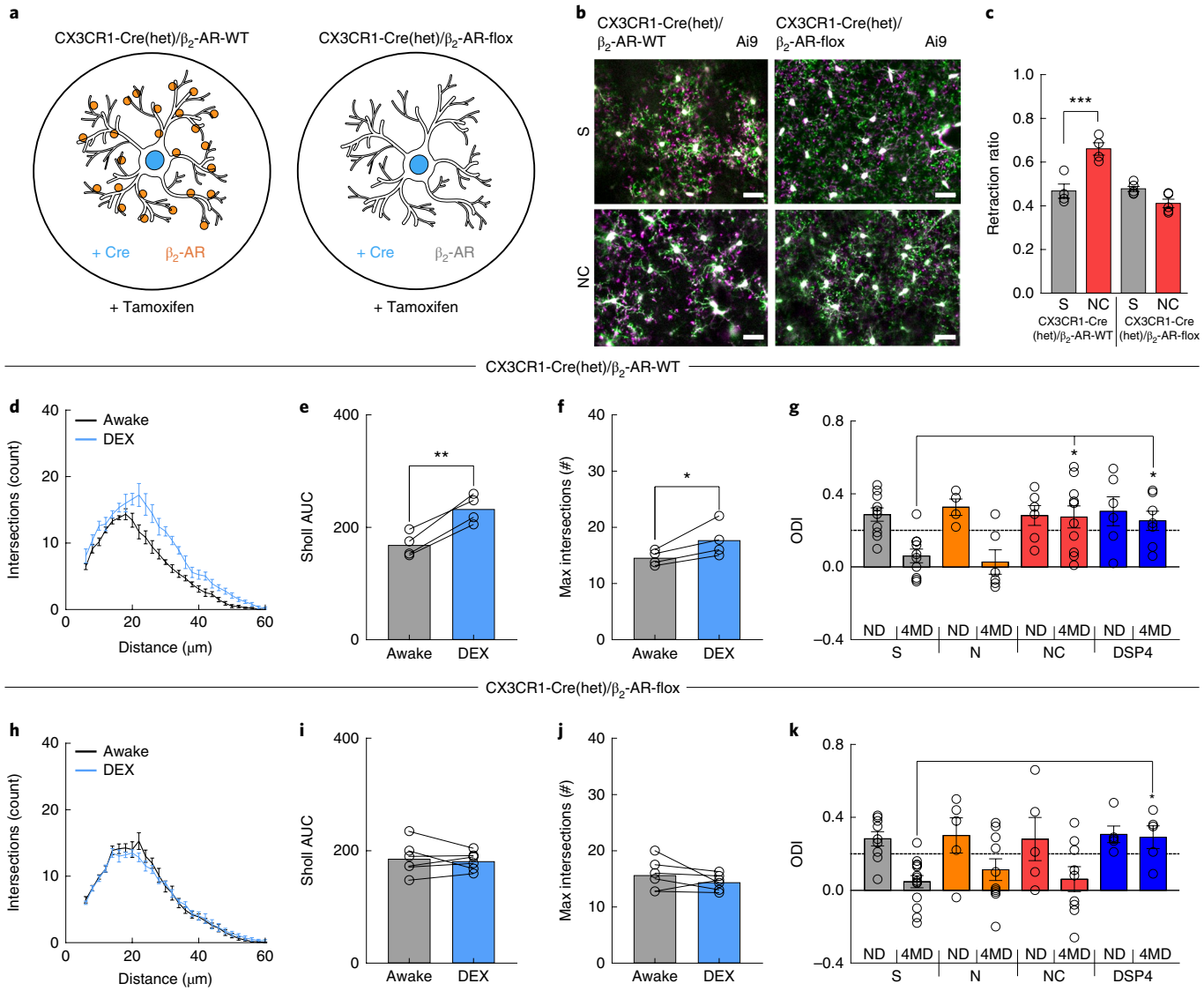

Fig. 7 | Microglial β_2-ARs mediate the effects of clenbuterol on ODP. a, Schematic of the transgenic lines used to generate microglia with and without β_2-ARs (orange circles). **b**, Example overlays of microglia at $t = 0$ min (magenta) and $t = 30$ min (green) in CX3CR1-Cre^{ERT}(het)/Ai9 and CX3CR1-Cre^{ERT}(het)/b$_2$-AR-flox/Ai9 mice after treatment with saline or with nadolol and clenbuterol. Note the absence of increased retraction (magenta) after treatment with nadolol and clenbuterol in microglia lacking β_2-ARs. **c**, Ablation of microglial β_2-ARs prevents pseudopodia retraction induced by nadolol and clenbuterol ($n = 4$ (Cre/Ai9 + S), 4 (Cre/Ai9 + NC), 5 (Cre/B2/Ai9 + S) and 5 (Cre/B2/Ai9 + NC) mice; two-way RM-ANOVA: significant main effects of genotype ($P = 0.00083$, $F(1,7) = 31.22$), treatment ($P = 0.035$, $F(1,7) = 6.77$) and interaction ($P = 0.0011$, $F(1,7) = 28.56$); Holm–Sidak multiple comparisons: Cre/Ai9 + S versus Cre/Ai9 + NC, $P = 0.0022$). **d**, Sholl profiles of awake (black) and DEX-treated (blue) CX3CR1-Cre^{ERT}(het)/Ai9 mice ($n = 4$ mice, 3–5 microglia per mouse). **e**,**f**, DEX treatment increases the Sholl AUC ($n = 4$ mice; two-sided paired t-test, $P = 0.0033$, $t(3) = 8.61$) (**e**) and the maximum Sholl intersections ($n = 4$ mice; two-sided paired t-test, $P = 0.047$, $t(3) = 3.27$) (**f**). **g**, Quantification of the ODI in CX3CR1-Cre^{ERT}(het) mice demonstrates robust ocular dominance shifts in mice with saline and nadolol treatment but no shifts in mice with nadolol and clenbuterol or DSP4 treatment ($n = 10$ (S + ND), 9 (S + 4MD), 4 (N + ND), 5 (N + 4MD), 6 (NC + ND), 10 (NC + 4MD), 6 (DSP4 + ND) and 7 (DSP4 + 4MD) mice; two-way ANOVA: significant main effect of monocular deprivation ($P = 0.00067$, $F(1,51) = 13.12$) and interaction ($P = 0.045$, $F(3,51) = 2.88$); Holm–Sidak multiple comparisons: S + 4MD versus NC + 4MD, $P = 0.0067$; S + 4MD versus DSP4 + 4MD, $P = 0.022$). **h**–**j**, Sholl profiles of awake (black) and DEX-treated (blue) CX3CR1-Cre^{ERT}(het)/b$_2$-AR-flox/Ai9 mice show similar microglial process arborization ($n = 6$ mice, 3–5 microglia per mouse) (**h**) with no changes in Sholl AUC ($n = 6$ mice; two-sided paired t-test, $P = 0.63$, $t(5) = 0.51$) (**i**) or the maximum Sholl intersections ($n = 6$ mice; two-sided paired t-test, $P = 0.27$, $t(5) = 1.23$) (**j**). **k**, Quantification of ODI in CX3CR1-Cre^{ERT}(het)/b$_2$-AR-flox mice. Ablation of microglial β_2-ARs rescues plasticity in mice treated with nadolol and clenbuterol but not in DSP4-treated mice ($n = 9$ (S + ND), 15 (S + 4MD), 5 (N + ND), 9 (N + 4MD), 5 (NC + ND), 9 (NC + 4MD), 5 (DSP4 + ND) and 5 (DSP4 + 4MD) mice; two-way ANOVA: main effect of MD ($P = 0.00080$, $F(1,54) = 12.62$); Holm–Sidak multiple comparisons: S + 4MD versus DSP4 + 4MD, $P = 0.046$). Scale bar, 20 μm. Graphs show mean ±s.e.m.; $^*P < 0.05$, $^{**}P < 0.01$, $^{***}P < 0.005$. Points represent individual animals. See Supplementary Table 1 for the numbers of females and males used in these experiments.

could make astrocytes an intermediary by which depletion of NE may be altering both microglial function and neural plasticity. It is also important to note that other signaling pathways affected by NE may also affect microglia. The regulation of glymphatic flow by wakefulness, for instance, may be an additional mechanism by which NE signaling in other cell types may influence microglial

dynamics, in this case by altering extracellular space[16], although the extent to which extracellular space increases during wakefulness remains unclear[34].

Intracellular signaling effectors of β_2-AR in microglia. β_2-AR and $P2Y_{12}$ signaling have opposite effects on microglial morphology, chemotaxis[35] and ODP. Both receptors are G-protein coupled. Whereas $P2Y_{12}$ is coupled to the G_i subunit, the β_2-AR is coupled to G_s, suggesting that these may act in a push–pull system[24] (Supplementary Fig. 15). The intracellular pathways that mediate G-protein signaling in microglia have recently garnered interest. Ex vivo, β_2-AR stimulation by NE and β_2-AR agonists blocks $P2Y_{12}$ process chemotaxis toward ATP by downstream protein kinase A-dependent phosphorylation of phosphoinositide 3-kinase g (refs. [24,36]), suggesting that this pathway may be important. Interestingly, downstream cyclic AMP has been elucidated as a key regulator of the dynamic shifts in microglial processes between filopodial and pseudopodial protrusions[22]. Microglial G_s-coupled receptors, including β_2-ARs, promote cyclic AMP accumulation, thereby driving a filopodial-rich phenotype that alters microglial dynamics and surveillance[22]. Recent studies in acute brain slices showed that baseline microglial motility relies on maintenance of microglial resting membrane potential by the two-pore-domain channel THIK-1 (refs. [37,38]). Genetic or pharmacologic perturbations of THIK-1 function reduce microglial ramification and surveillance, similarly to β_2-AR stimulation, making it another likely target. Although $P2Y_{12}$ signaling does not alter basal surveillance in microglia, it does gate THIK-1 function, causing hyperpolarization in response to ATP. β_2-ARs could similarly interface with THIK-1 or Kir K^+ channels to alter the microglial resting membrane potential, thereby inhibiting surveillance. This is the case in neurons of the medial prefrontal cortex, where clenbuterol hyperpolarizes fast-spiking GABAergic interneurons[39] as a result of β_2-AR-driven $G\alpha_s$ inhibition of inward Kir K^+-rectifying channels. β_2-ARs could also regulate microglial motility through recruitment and signaling by β-arrestin1 and β-arrestin2, which are both expressed in mouse microglia[40] and can have diverse downstream targets, including cytoskeletal proteins[41]. Recent work in zebrafish showed a critical role of β-arrestin1 in maintaining normal microglial morphology, surveillance and phagocytosis[42]. Long-term activation of β_2-ARs can lead to heterologous desensitization and possible endocytosis of other GPCRs such as $P2Y_{12}$ (ref. [41]) through β-arrestins. Activation of β-arrestin2 in microglia initiates longer-term anti-inflammatory signaling through blockade of mitogen-activated protein kinases, rescuing neuronal death in a Parkinson's disease model[43]. $P2Y_{12}$ signaling can also drive IL-1β production and inflammasome recruitment in response to lipopolysaccharide (LPS)-triggered inflammation[37], suggesting that cytokine effectors may critically alter the microglial and inflammatory milieu after activation of GPCRs. It is important to note that many forms of plasticity[44], including ODP[45], are thought to be mediated by cytokines, such as IL-1β and tumor necrosis factor-α, which are also known to promote sleep[46]. If microglial β_2-AR signaling is also regulated by sleep–wake cycles, then microglial β_2-ARs may in turn also alter sleep through regulation of cytokine production driven by downstream nuclear factor-kβ signaling[47]. It is important to note that most of our experiments were carried out in mice haploinsufficient for CX3CR1. Although CX3CR1 loss does not affect microglial morphology, motility, contact with synapses or ODP[48], interactions between NE and fractalkine signaling have been reported[49], making it possible that the effects of NE may be more or less pronounced in wild-type mice. Additionally, although the pharmacologic agents used were highly specific, off-target effects are always possible. However, previous work and our findings paint an emerging picture of a delicate interplay between $P2Y_{12}$ and β_2-AR signaling that mediates the responsivity of microglia to acute perturbations in the CNS milieu.

We explored the effects of β_2-AR signaling on microglial physiology, and the diversity of intracellular signaling pathways downstream of microglial β_2-ARs makes this receptor a fascinating target for the gating of microglial physiology and responses in the context of disease. Sleep disturbances are a hallmark of neurodegenerative diseases[50]. Interestingly, prolonged wakefulness and increased noradrenergic signaling prevent adequate astrocyte-driven glymphatic clearance of amyloid β (ref. [16]). We found that acute noradrenergic signaling inhibits microglial recruitment to acute tissue damage, and NE may be helpful in mediating microglial responses to chronic degenerative disease states. Although more work is needed to understand NE's role in mediating microglial function in health and disease, altogether, our data show that microglial β_2-ARs are potent regulators of microglial dynamics and visual system experience-dependent plasticity. Our study provides promising evidence that microglia have critically different roles in the anesthetized and awake brain.

Online content

Any methods, additional references, Nature Research reporting summaries, source data, statements of code and data availability and associated accession codes are available at https://doi.org/10.1038/s41593-019-0514-0.

Received: 20 February 2019; Accepted: 12 September 2019;
Published online: 21 October 2019

References

1. Schafer, D. P., Lehrman, E. K. & Stevens, B. The 'quad-partite' synapse: microglia–synapse interactions in the developing and mature CNS. *Glia* **61**, 24–36 (2013).
2. Nimmerjahn, A., Kirchhoff, F. & Helmchen, F. Resting microglial cells are highly dynamic surveillants of brain parenchyma in vivo. *Science* **308**, 1314–1318 (2005).
3. Davalos, D. et al. ATP mediates rapid microglial response to local brain injury in vivo. *Nat. Neurosci.* **8**, 752–758 (2005).
4. Tremblay, M. E., Lowery, R. L. & Majewska, A. K. Microglial interactions with synapses are modulated by visual experience. *PLoS Biol.* **8**, e1000527 (2010).
5. Miyamoto, A. et al. Microglia contact induces synapse formation in developing somatosensory cortex. *Nat. Commun.* **7**, 12540 (2016).
6. Wake, H., Moorhouse, A. J., Jinno, S., Kohsaka, S. & Nabekura, J. Resting microglia directly monitor the functional state of synapses in vivo and determine the fate of ischemic terminals. *J. Neurosci.* **29**, 3974–3980 (2009).
7. Stowell, R. D. et al. Cerebellar microglia are dynamically unique and survey Purkinje neurons in vivo. *Dev. Neurobiol.* **78**, 627–644 (2018).
8. Schafer, D. P. et al. Microglia sculpt postnatal neural circuits in an activity and complement-dependent manner. *Neuron* **74**, 691–705 (2012).
9. Parkhurst, C. N. et al. Microglia promote learning-dependent synapse formation through brain-derived neurotrophic factor. *Cell* **155**, 1596–1609 (2013).
10. Sipe, G. O. et al. Microglial $P2Y_{12}$ is necessary for synaptic plasticity in mouse visual cortex. *Nat. Commun.* **7**, 10905 (2016).
11. Paolicelli, R. C. et al. Synaptic pruning by microglia is necessary for normal brain development. *Science* **333**, 1456–1458 (2011).
12. Hoshiko, M., Arnoux, I., Avignone, E., Yamamoto, N. & Audinat, E. Deficiency of the microglial receptor CX3CR1 impairs postnatal functional development of thalamocortical synapses in the barrel cortex. *J. Neurosci.* **32**, 15106–15111 (2012).
13. Zhan, Y. et al. Deficient neuron–microglia signaling results in impaired functional brain connectivity and social behavior. *Nat. Neurosci.* **17**, 400–406 (2014).
14. Dissing-Olesen, L. et al. Activation of neuronal NMDA receptors triggers transient ATP-mediated microglial process outgrowth. *J. Neurosci.* **34**, 10511–10527 (2014).
15. Ding, F. et al.α1-adrenergic receptors mediate coordinated Ca^{2+} signaling of cortical astrocytes in awake, behaving mice. *Cell Calcium* **54**, 387–394 (2013).
16. Xie, L. et al. Sleep drives metabolite clearance from the adult brain. *Science* **342**, 373–377 (2013).
17. Yang, G. et al. Sleep promotes branch-specific formation of dendritic spines after learning. *Science* **344**, 1173–1178 (2014).
18. Aton, S. J. et al. Mechanisms of sleep-dependent consolidation of cortical plasticity. *Neuron* **61**, 454–466 (2009).

19. O'Donnell, J., Zeppenfeld, D., McConnell, E., Pena, S. & Nedergaard, M. Norepinephrine: a neuromodulator that boosts the function of multiple cell types to optimize CNS performance. *Neurochem. Res.* **37**, 2496–2512 (2012).
20. Zhang, Y. et al. An RNA-sequencing transcriptome and splicing database of glia, neurons, and vascular cells of the cerebral cortex. *J. Neurosci.* **34**, 11929–11947 (2014).
21. Nelson, L. E. et al. The α_2-adrenoceptor agonist dexmedetomidine converges on an endogenous sleep-promoting pathway to exert its sedative effects. *Anesthesiology* **98**, 428–436 (2003).
22. Bernier, L. P. et al. Nanoscale surveillance of the brain by microglia via cAMP-regulated filopodia. *Cell Rep.* **27**, 2895–2908 (2019).
23. Bellesi, M., Tononi, G., Cirelli, C. & Serra, P. A. Region-specific dissociation between cortical noradrenaline levels and the sleep/wake cycle. *Sleep* **39**, 143–154 (2016).
24. Gyoneva, S. & Traynelis, S. F. Norepinephrine modulates the motility of resting and activated microglia via different adrenergic receptors. *J. Biol. Chem.* **288**, 15291–15302 (2013).
25. Frenkel, M. Y. & Bear, M. F. How monocular deprivation shifts ocular dominance in visual cortex of young mice. *Neuron* **44**, 917–923 (2004).
26. Gordon, J. A. & Stryker, M. P. Experience-dependent plasticity of binocular responses in the primary visual cortex of the mouse. *J. Neurosci.* **16**, 3274–3286 (1996).
27. Kasamatsu, T. & Pettigrew, J. D. Depletion of brain catecholamines: failure of ocular dominance shift after monocular occlusion in kittens. *Science* **194**, 206–209 (1976).
28. Pettigrew, J. D. & Kasamatsu, T. Local perfusion of noradrenaline maintains visual cortical plasticity. *Nature* **271**, 761–763 (1978).
29. Hinoi, E. et al. The sympathetic tone mediates leptin's inhibition of insulin secretion by modulating osteocalcin bioactivity. *J. Cell Biol.* **183**, 1235–1242 (2008).
30. Toth, L. A. & Bhargava, P. Animal models of sleep disorders. *Comp. Med.* **63**, 91–104 (2013).
31. Wulff, K., Gatti, S., Wettstein, J. G. & Foster, R. G. Sleep and circadian rhythm disruption in psychiatric and neurodegenerative disease. *Nat. Rev. Neurosci.* **11**, 589–599 (2010).
32. Polack, P. O., Friedman, J. & Golshani, P. Cellular mechanisms of brain state-dependent gain modulation in visual cortex. *Nat. Neurosci.* **16**, 1331–1339 (2013).
33. Frank, M. G., Issa, N. P. & Stryker, M. P. Sleep enhances plasticity in the developing visual cortex. *Neuron* **30**, 275–287 (2001).
34. Smith, A. J., Yao, X., Dix, J. A., Jin, B. J. & Verkman, A. S. Test of the 'glymphatic' hypothesis demonstrates diffusive and aquaporin-4-independent solute transport in rodent brain parenchyma. *eLife* **6**, e27679 (2017).
35. Sipe, G. O. et al. Microglial P2Y12 is necessary for synaptic plasticity in mouse visual cortex. *Nat. Commun.* **7**, 10905 (2016).
36. Schneble, N. et al. Phosphoinositide 3-kinase γ ties chemoattractant- and adrenergic control of microglial motility. *Mol. Cell Neurosci.* **78**, 1–8 (2016).
37. Madry, C. et al. Microglial ramification, surveillance, and interleukin-1β release are regulated by the two-pore domain K^+ channel THIK-1. *Neuron* **97**, 299–312 (2018).
38. Madry, C. et al. Effects of the ecto-ATPase apyrase on microglial ramification and surveillance reflect cell depolarization, not ATP depletion. *Proc. Natl Acad. Sci. USA* **115**, E1608–E1617 (2018).
39. Luo, F. & Zhou, H. Clenbuterol reduces GABAergic transmission in prefrontal cortex layer 5/6 pyramidal neurons of juvenile rat via reducing action potentials firing frequency of GABAergic interneurons. *J. Neurochem.* **144**, 152–161 (2018).
40. Guneykaya, D. et al. Transcriptional and translational differences of microglia from male and female brains. *Cell Rep.* **24**, 2773–2783 (2018).
41. Smith, J. S. & Rajagopal, S. The β-Arrestins: multifunctional regulators of G protein-coupled receptors. *J. Biol. Chem.* **291**, 8969–8977 (2016).
42. Li, Y., Du, X., Pei, G., Du, J. & Zhao, J. β-arrestin1 regulates the morphology and dynamics of microglia in zebrafish in vivo. *Eur. J. Neurosci.* **43**, 131–138 (2016).
43. Qian, L. et al. β_2-adrenergic receptor activation prevents rodent dopaminergic neurotoxicity by inhibiting microglia via a novel signaling pathway. *J. Immunol.* **186**, 4443–4454 (2011).
44. Labrousse, V. F. et al. Impaired interleukin-1β and c-Fos expression in the hippocampus is associated with a spatial memory deficit in $P2X_7$ receptor-deficient mice. *PLoS One* **4**, e6006 (2009).
45. Kaneko, M., Stellwagen, D., Malenka, R. C. & Stryker, M. P. Tumor necrosis factor-α mediates one component of competitive, experience-dependent plasticity in developing visual cortex. *Neuron* **58**, 673–680 (2008).
46. Krueger, J. M., Obal, F. J., Fang, J., Kubota, T. & Taishi, P. The role of cytokines in physiological sleep regulation. *Ann. N. Y. Acad. Sci.* **933**, 211–221 (2001).
47. Kolmus, K., Tavernier, J. & Gerlo, S. β_2-adrenergic receptors in immunity and inflammation: stressing NF-κB. *Brain Behav. Immun.* **45**, 297–310 (2015).
48. Lowery, R. L., Tremblay, M. E., Hopkins, B. E. & Majewska, A. K. The microglial fractalkine receptor is not required for activity-dependent plasticity in the mouse visual system. *Glia* **65**, 1744–1761 (2017).
49. Madrigal, J. L., Caso, J. R., Garcia-Bueno, B., Gutierrez, I. L. & Leza, J. C. Noradrenaline induces CX3CL1 production and release by neurons. *Neuropharmacology* **114**, 146–155 (2017).
50. Musiek, E. S. & Holtzman, D. M. Mechanisms linking circadian clocks, sleep, and neurodegeneration. *Science* **354**, 1004–1008 (2016).

Acknowledgements

We thank the University of Rochester Medical Center Flow Core for their expert training and services. We thank C. Lamantia for assistance with animal management; J. Olschowka and K. O'Banion for shared PCR resources; F. Rivera-Escalera for providing training on tissue preparation for microglial FACS; A. Ghosh for the Sholl analysis ImageJ plugin; and J. Cang for sharing MATLAB code for OD analysis. This work was supported by National Institutes of Health grants R01 EY019277 (A.K.M.), R21 NS099973 (A.K.M.), R01 AA027111 (A.K.M.), R01 EY028219 (M.S.), F31 NS105249 (R.D.S.), T32 NS007489 (R.D.S., G.O.S.), F31 NS086241 (G.O.S.) and F32 EY028028 (G.O.S.); National Science Foundation grant NSF 1557971 (A.K.M.); a Schmitt Program on Integrative Brain Research grant (G.O.S. and R.P.D.); the University of Rochester Bilski-Mayer Fellowship (H.N.B.); and the University of Rochester Medical Center Summer Scholars Fellowship (K.A.L.).

Author contributions

R.D.S., G.O.S. and A.K.M. conceived the project. R.D.S., G.O.S., R.P.D., H.N.B., K.A.L., B.S.W. and M.B.S. carried out experiments and data analysis. R.D.S. carried out iOS imaging experiments and analysis in CX3CR1-Cre^{ERT}/β_2-AR-flox, CX3CR1-Cre^{ERT} and C57BL/6J mice, all in vivo two-photon experiments characterizing awake versus anesthetized mice and adrenergic pharmacologic agents, and imaging experiments using CX3CR1-Cre^{ERT}/β_2-AR-flox/Ai9 and CX3CR1-Cre^{ERT}/Ai9 mice. R.D.S. also performed all FACS preparation on microglial specimens. G.O.S. carried out iOS imaging experiments in C57BL/6J mice and imaging experiments characterizing stress and circadian rhythms. G.O.S. also performed experiments using terbutaline. G.O.S. performed all resonance imaging and optogenetic experiments. R.P.D. carried out stress experiments. H.N.B. assisted in confirmation of CX3CR1-Cre/β_2-AR-flox excision and DSP4 depletion histology experiments. K.A.L. carried out circadian morphology experiments. B.S.W. performed all slice experiments. M.B.S. assisted with DSP4 histology experiments and CX3CR1-Cre/β_2-AR-flox expression histology. J.M.B. contributed to the design of experiments with pharmacologic agents. E.B. advised on the design and analysis of stress experiments. M.S. advised on the design and analysis of optogenetic and resonance imaging experiments. R.D.S., G.O.S. and A.K.M. wrote the first draft of the manuscript. All authors contributed to the final version of the manuscript.

Competing interests

The authors declare no competing interests.

Additional information

Supplementary information is available for this paper at https://doi.org/10.1038/s41593-019-0514-0.

Correspondence and requests for materials should be addressed to A.K.M.

Methods

Animals. Experimental protocols were carried out with the approval of the Institutional Animal Care and Use Committees of both the University of Rochester and Massachusetts Institute of Technology and conformed to National Institutes of Health guidelines. Experiments were conducted on male and female mice with a C57BL/6 background between P21 and P120. CX3CR1^{GFP} (ref. [51]; JAX 005582) heterozygous mice were used to visualize microglia for in vivo two-photon imaging. CX3CR1^{GFP} mice were also crossed to THY1-YFP[52] (JAX 003782) mice to visualize both microglia and dendritic spines for spine contact imaging. CX3CR1-Cre^{ERT} (ref. [9]; JAX 021160) mice were bred to b_2-AR-flox[29] (Karsenty laboratory, courtesy of the Rosen laboratory) mice to generate mice that had β_2-ARs selectively knocked out of microglia. CX3CR1-Cre^{ERT} mice were also bred to Ai9[53] (tdTomato; JAX 007909) mice for visualization of microglia in two-photon experiments. Mice were housed with a standard 12-h light/12-h dark cycle and fed standard chow ad libitum. For experiments regarding ODP, mice were used in the visual critical period (P25–P35). Sex distribution is provided in Supplementary Table 1, but numbers for all experiments can be found in the figure legends. More information can be found in the Life Sciences Reporting Summary.

Stress exposure. For stress exposure experiments, male and female mice were randomly assigned to control or stressed cohorts. Stressed mice were briefly anesthetized using 3% isoflurane and restrained in 50-ml conical tubes drilled with air holes in a brightly lit fume hood for 2 h. This stress period was repeated for three consecutive days at approximately the same time each day. After the third day, mice were imaged either immediately after the final stressor or 4 h after the final stressor. Control mice were handled on each day but returned to their home cages.

Circadian rhythm measurements. For circadian rhythm experiments, mice were kept on the standard 12-h light/12-h dark cycle with lights on at 6:00 and lights off at 18:00. For fixed-tissue analysis, brains were collected at 6:00, 12:00, 18:00 and 24:00. For in vivo experiments, animals were imaged at 12:00 and 24:00. For collection times during the dark cycle, cages were covered with a black sheet to minimize light exposure before experiments.

Flow isolation of microglia and confirmation of β_2-AR excision. We used our previously published experimental design[54] with a small modification to accommodate the YFP expression in the CX3CR1-Cre^{ERT} line. CX3CR1-Cre^{ERT}/β_2-AR-flox mice were either dosed with 50 µg tamoxifen from P2 to P4 or undosed. At ~P28, mice were killed by an intraperitoneal sodium pentobarbital overdose (Euthasol; Virbac) and transcardially perfused with ice-cold 0.15 M PBS. Each brain was removed, and the whole cortex was dissected from the rest of the brain in ice-cold, degassed fluorescence-activated cell sorting (FACS) buffer (0.5% BSA (Sigma, A2153) in 1× PBS (Invitrogen, 20012-027), pH 7.2). The tissue was kept on ice throughout all the procedures. Cortices were homogenized with a Dounce homogenizer and then passed through a 70-µm filter and centrifuged (210*g*, 7 min, 4 °C). The supernatant was aspirated from the pellets, and the pellets were resuspended and prepared for magnetic sorting with Myelin Removal Beads II (Miltenyi, 130-0960733). The resuspended labeled tissue was passed through a 70-µm filter and then the FACS buffer-primed magnetic columns (Miltenyi, 130-096-733). After passage through the magnetic columns, the samples were centrifuged, and the supernatant was removed and resuspended in FACS buffer with Fc block (BioLegend, 101320) for 15 min at 4 °C.

Samples were incubated with anti-CD11b-AlexaFluor BV786 (1:200; BD Biosciences, 740861, clone M1/70) and anti-CD45-APC (1:400; BD Biosciences, 561018, clone 30-F11) for 30 min in the dark at 4 °C. Each sort included the following compensation controls: BV720 bead control, APC bead control (eBiosciences, 01-111-42), unstained live cells and propidium iodide (PI)-labeled Triton X-100-killed cells. An additional fully labeled sample was prepared with spare tissue to check the voltage settings before running experimental samples. All samples were run on an 18-color FACSAria II flow cytometer. For the sort, all samples and controls were resuspended in 300 µl of FACS buffer. PI was added to the samples just before sorting. An example of a microglial sort can be found in Supplementary Fig. 8. More information can be found in the Life Sciences Reporting Summary.

Cells were collected in PBS for DNA isolation with a Qiagen DNAeasy DNA isolation kit. A total of three tamoxifen-treated and three tamoxifen-untreated animals were included in our confirmation experiments. Isolated DNA was run through two PCR protocols: first, the PCR for confirmation of floxed allele presence (550-bp product: Fw, ccaaagttgttgcacgtcac; Rv, gcacacgccaaggagattat); and second, excision confirmation (~800-bp product: Fw, ccaaagttgttgcacgtcac; Rv, aagaaagaggaggggctgag)[29]. We confirmed that in tamoxifen-treated mice the 550-bp floxed allele PCR product was no longer present (Supplementary Fig. 8) and the excision product of ~800 bp was present. In our untreated mice, we still had the 550-bp floxed allele; however, we did also see the ~800-bp excision product in the second PCR. This suggests that there was a certain degree of leakiness in our Cre expression. However, this leakiness did not affect our experimental outcomes, as our controls for all CX3CR1-Cre^{ERT}/b_2-AR-flox experiments were CX3CR1-Cre^{ERT}(het) mice dosed with tamoxifen.

Pharmacologic agents. Fentanyl cocktail[4,7,10,48] comprised fentanyl (0.05 mg per kg, intraperitoneally), midazolam (5.0 mg per kg, intraperitoneally) and DEX (0.5 mg per kg) premixed and given intraperitoneally and was used for anesthetized two-photon imaging sessions and for thin-skull and cranial window procedures. DEX[21] solution contained 0.4 mg per kg DEX and was given intraperitoneally for two-photon imaging. Atipamizole solution contained 0.2 mg per kg atipamizole given intraperitoneally and was used to reverse DEX anesthesia.

Clenbuterol[55] (Sigma, 21898-19-1) solution contained 1–5 mg per kg clenbuterol administered intraperitoneally for two-photon imaging and 5 mg per kg clenbuterol administered intraperitoneally once every 12 h for 4 d for iOS. Nadolol[56] (Sigma, 42200-33-9) solution contained 10 mg per kg nadolol administered intraperitoneally for two-photon imaging and once every 12 h for 4 d for iOS. ICI-118,551 (ref. [57]; Sigma, 72795-01-8) solution contained 10 mg per kg ICI-118,551 administered intraperitoneally for two-photon imaging and 8 mg per kg daily by mini-osmotic pump for 4 d (Alzet, 1007D) for iOS. DSP4 (ref. [58]; Sigma, 40616-75-9) solution contained 50 mg per kg DSP4 administered intraperitoneally twice at 48-h intervals a minimum of 48 h before either two-photon imaging or the deprivation period of intrinsic optical signal imaging (iOS). Tamoxifen (Sigma, 10540-29-1; 50 µg) was administered by intragastric gavage once daily from ~P2–P4 in experiments using CX3CR1-Cre^{ERT} mice[9].

Monocular deprivation. Animals were randomly assigned to ND or 4MD cohorts starting from P27 ± 2 d. MD animals were anesthetized (isoflurane: 5% for induction, 3% for maintenance). The right eyelids were trimmed, and antibiotic eye ointment was applied to the eye and trimmed margins. The eye was then sutured closed. Mice were monitored and given carprofen (5 mg per kg) every 24 h for analgesia as needed. The eye was not reopened until the day of imaging, and any animals with a compromised eye or sutures were excluded from the rest of the experiment.

iOS imaging. These experiments used C57BL/6, CX3CR1-Cre^{ERT}(het) and CX3CR1-Cre^{ERT}(het)/b_2-AR-flox mice. After 4 d of ND or MD, animals were re-anaesthetized with isoflurane and chloroproxithene (2 mg per kg), and sutured eyes were reopened. The skull over the contralateral visual cortex was exposed, cleared, covered with agarose (0.25%) and sealed with a coverslip. Animal anesthesia was maintained with isoflurane (0.75%) throughout imaging. A custom-made iOS imaging setup was used to record activity in the visual cortex during presentation of a visual stimulus (DALSA 2M30 CCD). The cortex was illuminated with 550-nm light to identify vasculature and 700-nm light for iOS collection. Images of the left visual cortex were collected continuously while either the ipsilateral or contralateral eye was stimulated by white horizontal square-wave bar gratings on a black background moving upward (90˚) or downward (270˚) at a frequency of 8˚ s^{-1} for 6 min (30 cm from the eyes). Visually evoked responses were collected for each eye individually. The normalized amplitude of the fast Fourier transform component of the intrinsic signal was averaged for each eye from responses to both stimulus directions and compared between eyes offline using MATLAB to determine ocular dominance. An ODI was computed using the following equation: ODI = (average contralateral response – average ipsilateral response)/(average contralateral response/average ipsilateral response).

Acute cortical slice preparation. CX3CR1-^{GFP}(het) mice were decapitated, and the brain was rapidly removed and placed into ice-cold artificial cerebrospinal fluid (ACSF) containing (in mM) 126 NaCl, 2.5 KCl, 1.25 KH_2PO_4, 10 glucose, 1.3 $MgSO_4$, 26 $NaHCO_3$ and 2.5 $CaCl_2$ and constantly oxygenated (95% O_2, 5% CO_2). Coronal sections 400 µm in thickness were prepared using a vibratome (Vibratome 1000) with the brain submerged in ice-cold oxygenated ACSF. Sections containing visual cortex were transferred to oxygenated ACSF at ambient temperature until imaging (between 30 min and 2 h). Slices were placed in a perfusion chamber (Warner Instruments) and perfused with 1–2 ml min^{-1} oxygenated ACSF heated to 37 °C using an inline heater (Warner Instruments), and cortical GFP-expressing microglia were imaged at a depth of 50–100 µm below the surface using a two-photon microscope. An initial time series of *z* stacks was taken every 5 min for 30 min in slices perfused with ACSF. The perfusion solution was then switched to ACSF containing 100 nM DEX (Tocris) or normal ACSF, samples were allowed to incubate for 20 min and *z* stacks of the same area were taken every 5 min for 30 min. Motility was analyzed as described below.

Cranial window surgery. Animals were anesthetized using the fentanyl cocktail during the cranial window implantation surgical procedure. Lubricant ointment was used to keep the eyes moist and protected. Body temperature was maintained at 37 °C during the surgery. Aseptic technique was adhered to during all surgical procedures: all tools were autoclaved for steam sterilization, and tools were sterilized in a bead sterilizer between surgeries (up to three uses). Mice were mounted in a stereotaxic frame and head fixed for surgical procedures. The skull was exposed through a scalp incision, and all connective tissues were cleared off the skull. A 3-mm biopsy punch (Integra) was then used to create a circular score on the skull over V1. A 0.5-mm drill bit (FST) was used to then drill through the skull for the craniotomy, tracing the 3-mm score. A 5-mm coverslip attached to a 3-mm coverslip (Warner Instruments) by UV glue (Norland Optical Adhesive,

Norland) was then slowly lowered into the craniotomy (3-mm side down). The coverslip was carefully secured with Loctite 404 glue (Henkel). A custom headplate produced by emachine shop (http://www.emachineshop.com) (designs courtesy of the Mriganka Sur laboratory, Massachusetts Institute of Technology) was then secured onto the skull using C&B Metabond dental cement (Parkell). The cement was used to cover the rest of skull and seal the incision site. Animals were administered slow-release buprenex by University of Rochester Medical Center veterinary staff (5 mg per kg subcutaneously every 72 h) and monitored for 72 h postoperatively.

Two-photon microscopy. A custom two-photon laser-scanning microscope was used for in vivo imaging (Ti:Sapphire, Mai-Tai, Spectra Physics; modified Fluoview confocal scan head, ×20 lens, 0.95 NA, Olympus). Excitation for fluorescence imaging was achieved with 100-fs laser pulses (80 MHz) at 920 nm for GFP and 1,020 nm for tdTomato with a power of ~40 mW measured at the sample. For motility experiments in CX3CR1^{GFP} mice, a 580/180 (GFP) filter was used. For experiments in CX3CR1-Cre^{ERT}/Ai9 mice, a 578/105 filter was used. During anesthetized cranial window imaging sessions, mice were anesthetized with our fentanyl cocktail. Before awake imaging sessions, mice were trained for three consecutive days in a head restraint on a running wheel, progressing from 30 min to 1 h of head restraint over the 3 d. During awake imaging sessions, mice were head restrained and kept on a foam running wheel for the duration of the session. The restraint apparatus and wheel were the same as those used in the initial training sessions. During thin-skull[4,10,48] imaging sessions, mice were anesthetized with the fentanyl cocktail before the skull-thinning surgery and for the duration of the imaging session. During imaging sessions and during post-imaging recovery, mice were kept at 37 °C until they were alert. Imaging was conducted at ×3 to ×5 digital zoom with a 1-μm *z* step and time-lapse imaging was carried out at 5-min intervals over 1 h, with the exception of spine contact imaging, which was conducted at ×8 digital zoom. Image analysis was done offline using ImageJ and MATLAB with custom algorithms as described in Sipe et al.[10] and available on the Majewska laboratory website through GitHub.

Microglial morphology. For in vivo morphologic analysis, 3–5 microglia were selected per animal from a single time point in the imaging session. For paired time-course experiments using DEX and atipamezole, the same microglia were selected from the beginning of the first treatment condition and then 15 min into the second session. For all other experiments, microglia were selected from the same time point of the imaging sessions for consistency. For each microglia selected, an individual *z* projection was created in ImageJ, which encompassed the entire microglial arbor. All microglial processes were manually traced, and then the tracing of the processes was subjected to Sholl analysis. Because of the limits of manual tracing, small filopodia may have been missed. For each animal, an average of the 3–5 microglia selected was found, and that average represented the value for that animal. The AUC of the Sholl profile and then the maximum intersection number were found and analyzed as indices of microglial arbor complexity.

Microglial motility and surveillance. Microglial motility analysis was performed in ImageJ and MATLAB as previously described[7,10]. *z* stacks were collected in V1 every 5 min for 1 h, producing 12 time points. Data for the DEX time-course experiments were collected first with mice either awake or under DEX for 20 min and then 1 h immediately after DEX or atipamezole administration. All *z* stacks were between 60 and 120 μm, and for analysis average-intensity *z* projections were made (30–40 μm thick). Lateral motion artifacts and photobleaching were corrected for before analysis (Stackreg plugin, ImageJ). A custom MATLAB algorithm[7,10] was used to compare pixels across individual time points and across consecutive time points to generate a motility index (defined as the sum of all changed pixels divided by the unchanged pixels). Our motility script in MATLAB compares consecutive time points across the 5-min imaging intervals and calculates differences in pixels: pixels present in the first time point and absent in the second time point are defined as retractions; pixels absent in the first time point and appearing in the second time point are defined as extensions. The retractions and extensions are summed and divided by the stable pixels for each of these consecutive time point pairs to generate motility indices for each of the pairs. The final motility index that we show for our conditions represents the average of the motility indices calculated for each of the pairs. For the motility index, all microglia in the *z* projection of the imaging session were analyzed to generate the value per animal for the 1-h session. The thresholded time points were also used to calculate the area monitored (surveillance measurement) by microglia during the 1-h imaging session. This was done by collapsing the 12 time points through the maximum-intensity *z*-projection function in ImageJ and calculating the total number of pixels representing microglia of the total pixels in the field of view. The surveillance ratio was defined as the ratio of microglia-occupied pixels of the total pixels in the image.

Microglial pseudopodia measurements. For pseudopodia analysis, time points at t = 0, 30 and 60 min from the motility imaging sessions were used to create overlays for 0–30 and 30–60 min. The number of pseudopodia was then counted using the multipoint tool in ImageJ to track marked pseudopodia. Pseudopodia were identified as round, bulbous projections with a width greater than that of the parent processes from which they protruded (typically ~2–3 μm in diameter). Conversely, filopodia were identified as thin, acute processes tapered at the tip with a width less than of the parent process (typically <1 μm in width). Pseudopodia were identified for counting on the basis of their round morphology and their presence at the end-tips of processes. Retraction (retracted pseudopodia/total pseudopodia) and extension (extended pseudopodia/total pseudopodia) ratios were calculated on the basis of the number of retracted or extended pseudopodia divided by the total number of pseudopodia counted. Because comparisons were made over 30 min (overlays of 0–30 and 30–60 min), and pseudopodia are transient, all pseudopodia fell into the category of either retracted (magenta in Fig. 3a) or extended (green in Fig. 3a), providing a clear measurement of the tendency of processes to either extend or retract after treatment. For imaging of Ai9 animals, only the time points at 0 and 30 min were taken, as the tdTomato fluorophore suffered from pronounced photobleaching with repeated imaging. This precluded the use of Ai9 mice for motility measurements.

Terbutaline motility. For direct application of terbutaline to the brain parenchyma, small craniotomies were performed on anesthetized animals and imaged directly without a coverslip. Baseline imaging data were collected every 2 min for 30 min in a sterile saline objective immersion. After baseline imaging data were collected, the immersion medium was replaced by either additional sterile saline or terbutaline in sterile saline (1 mM) to allow for pharmacologic diffusion into the brain parenchyma and mice were imaged for an additional 60 min. Baseline periods and saline-treated animals controlled for microglial activation due to craniotomies, and animals that had significant motility or morphologic changes during baseline imaging were removed from the study.

Laser ablation. Laser ablation injuries were created out by running a point scan for 8 s at 780 nm using ~75 mW at the sample. The microglial injury response was imaged by collecting *z* stacks of 50–90 μm every 5 min. For analysis, *z* projections all comprised 10 μm of the stack, encompassing the approximate center ablation core. The file was converted to an .avi file and subjected to analysis by a custom MATLAB script designed to calculate the movement of microglial processes toward the ablation core. Briefly, for each pixel at each time point, the script generates a vector that estimates the magnitude and direction of motion of the pixel using the Farneback method for estimating optic flow[59]. To ensure that our analysis concentrated on the number and magnitude of responding processes, we excluded vectors not directed toward the core as well as vector magnitudes below 5 pixels of motion. This was necessary to filter out noise pixels that represent artifacts, such as motion and tissue distortion upon initial ablation. To quantify the generated vectors, we summed the magnitudes of all the vectors at each time point and normalized this value to the total number of pixels in the image. The first time point was excluded from all analysis, as the script estimates the first time point's movement by assuming a blank frame preceding the first time point. We then found the AUC for our injury-response-normalized magnitude as well as the maximum value of our normalized magnitude over the 1-h session.

Microglial–dendritic spine contact analysis. To visualize microglial contacts with dendritic spines, the GFP channel was assigned the color green and the YFP channel was assigned the color red. Microglial contacts with dendritic spines were identified by manually stepping through the *z* stack of the merged channels. Contact was identified as the colocalization of the fluorescence of microglial and dendritic elements. For each animal, 40–60 spines were evaluated for microglial contact (this represents the range of total spines typically visible for the duration of an entire imaging session). The proportion contacted spines in the analysis was quantified as the number of contacted spines out of the total spines counted.

Resonance imaging. Animals were head fixed and imaged using a ×16 objective with ×8 digital zoom at 38 frames per second and 8 raster averages, resulting in effectively 4 frames per second. A *z* piezo was used with a commercial two-photon microscope using proprietary software (Prairie View, Prairie Technologies, Bruker) to capture five planes that were 5 μm apart. Each stack was therefore captured at approximately 1.2 s at a resolution of 800 × 400 and using a Ti:Sapphire (Mai Tai) laser tuned to 910 nm. Baseline dynamics were captured for 15 min, followed by injection of DEX (300 μg per kg, subcutaneously) and immediate imaging for another 30 min. For analysis, 5-min averages were collected and overlaid as magenta and green for each time point pair. Pseudopodia and filopodia were counted in each frame and binned as either extension or retraction for each time. Process velocity and net distance were also computed using the manual tracking plugin (ImageJ).

Optogenetic stimulation of NE axons. CX3CR1^{GFP}/TH-Cre mice were generated and injected with 400 nl of AAV1-EF1a-double-flox-hChR2(H134R)-mCherry bilaterally in the LC. A cranial window was then created over V1. Viral expression was allowed to reach the cortex over 5 weeks before imaging. Animals were then injected with DEX (300 μg per kg) and allowed to sit in their home cage for 15 min before being head restrained and imaged. Frames were collected using a ×16 objective at 800 × 400 resolution with two frames averaged per *z* stack, resulting in

2.05 frames per second at ×4 digital zoom. Then, 40–60 *z* stacks were collected 5 µm apart at 910 nm. Baseline imaging was performed for 30 min without interlaced laser stimulation at ten 3-min intervals followed by 30 min of alternating laser stimulation (MBL-7-473-300 mW, Opto Engine, 473 nm, six 2-s pulses at 5 mW) over 60 s. This was followed by 90 s of imaging and 30 s of buffer time through the objective. CX3CR1^{GFP} mice without TH-Cre were subjected to the same imaging and light exposure paradigm and served as a light control for the optogenetic experiments.

Histology. Whole brains were collected after transcardial perfusion and overnight after fixation with paraformaldehyde (4%). Tissue was cryoprotected, and coronal sections were cut on a freezing microtome (Microm; Global Medical Instrumentation) at 50-µm thickness. Sections were processed free floating at room temperature (RT). Briefly, sections were rinsed, and endogenous peroxidase activity and nonspecific binding were blocked with a 10% BSA solution. Sections were then incubated in a primary antibody solution to detect microglial morphology in circadian experiments (24 h, 4 °C, anti-Iba-1, 1:1,000, Wako 019-19741) followed by secondary antibody solution (4 h, RT, AlexaFluor 488, 1:500, Invitrogen), mounted and coverslipped. For examination of microglial ramification in circadian rhythm experiments, sections containing primary visual cortex were identified and imaged on a Zeiss LSM 510 confocal microscope (Carl Zeiss). For each section, a 10-mm *z* stack in the center of the tissue was collected with a *z* step of 1 µm at ×40 magnification. Analysis was performed offline in ImageJ. *z* stacks were smoothed and compressed into a single *z* projection. For analysis of ramification, microglia whose entire process arbor was contained within the image were individually selected and cropped into a new image. In the circadian rhythm morphology study, 5 microglia from 3 fields of view, for a total of 15 microglia, were analyzed per animal. Each image was thresholded to generate a binarized outline of the process arbor, filtered to remove artifacts and analyzed with an automated Sholl analysis plugin (kindly provided by the Anirvan Ghosh laboratory, University of California, San Diego).

For analysis of noradrenergic fiber depletion after DSP4 administration, whole brains were collected from animals 48 h and 6 d after the second dose of DSP4. Tissue was processed for histology as described above. Sections were incubated in a primary antibody solution to label noradrenergic fibers[60] (overnight, 4 °C, anti-tyrosine hydroxylase, 1:400, Millipore 3122928, clone LNC1) followed by a secondary antibody solution (2 h, RT, AlexaFluor 594), mounted and coverslipped. Epifluorescent images of visual cortex-containing noradrenergic fibers were then collected using an Olympus Bx51 (Olympus, ×40/0.75 NA) with a Spot Pursuit digital camera and Spot Advanced software. Images were binarized in ImageJ to outline the fibers, using the average pixel intensity multiplied by 1.6 as a threshold value for binarization. The total number of white pixels was then measured. Results from 4–5 sections per animal were averaged.

For quantification of microglial labeling in CX3CR1-Cre^{ERT}/Ai9 mice, tissue was processed as above. Epifluorescent images of visual cortex with microglia in red were then collected using an Olympus Bx51 (Olympus, ×10/0.30 NA) with a Spot Pursuit digital camera and Spot Advanced software. Any white matter was cropped out of the image. Microglial cell bodies were marked in ImageJ using the paintbrush tool. Results from 4–5 sections per animal were averaged, with a correction for cropped area. Density was calculated as the number of microglia/area in visual cortex for tamoxifen-treated and control groups.

Corticosterone ELISA. Whole-trunk blood was collected in EDTA-lined tubes and centrifuged for 10 min at 3,000 r.p.m. at 4 °C. Plasma was aspirated from the pellet and stored at −20 °C until analyzed. Circulating plasma corticosterone was quantified using a competitive ELISA kit (EIACORT, ThermoFisher). Samples were run in duplicate and compared to a standard curve according to kit instructions. Final concentrations for each animal were the average of duplicate reads on a standard plate reader (iMark, Bio-Rad Laboratories).

Statistics. Statistical comparisons were made between animal cohorts using Prism VI statistical analysis software (GraphPad). No statistical methods were used to predetermine sample sizes, but our sample sizes were similar to those reported in previous publications from our lab[4,10,48] and other publications in the field. Numbers (*n*) were also chosen such that we could determine whether sex affected our experimental results; thus, sufficient males and females were included to meet this need. All *n* values represent individual animals. For analyses where multiple microglia were assayed per animal, all microglia analyzed for an individual animal were averaged to generate a single value per animal. Animals were randomly assigned to conditions with the caveat of an effort being made to evenly distribute males and females among the various groups. Where possible, in repeated imaging experiments, conditions were randomized to account for potential ordering effects. All analyses were conducted with blinding to the experimental condition. Animals were excluded from analysis only if an imaging session could not be completed in full; otherwise, all completed imaging sessions collected were used. All values reported are the mean ± s.e.m. For all analyses, $\alpha = 0.05$. Two-tailed unpaired or paired *t*-tests and one-way or two-way ANOVA with or without repeated measures (ANOVA and RM-ANOVA, respectively) with Holm–Sidak multiplicity-corrected post hoc comparisons were used to compare cohorts where appropriate. The data met the assumptions of normality and equal variances as tested by Prism VI as part of the statistical analyses. More information can be found in the Life Sciences Reporting Summary.

Reporting Summary. Further information on research design is available in the Nature Research Reporting Summary linked to this article.

Data availability

The data that support the findings of this study are available from the corresponding author upon reasonable request.

Code availability

MATLAB code for motility and laser ablation analysis is freely available at https://github.com/majewska-lab. More information can be found in the Life Sciences Reporting Summary.

References

51. Jung, S. et al. Analysis of fractalkine receptor CX(3)CR1 function by targeted deletion and green fluorescent protein reporter gene insertion. *Mol. Cell Biol.* **20**, 4106–4114 (2000).
52. Feng, G. et al. Imaging neuronal subsets in transgenic mice expressing multiple spectral variants of GFP. *Neuron* **28**, 41–51 (2000).
53. Madisen, L. et al. A robust and high-throughput Cre reporting and characterization system for the whole mouse brain. *Nat. Neurosci.* **13**, 133–140 (2010).
54. Wong, E. L. et al. Developmental alcohol exposure impairs synaptic plasticity without overtly altering microglial function in mouse visual cortex. *Brain Behav. Immun.* **67**, 257–278 (2018).
55. Ryan, K. M. et al. Clenbuterol activates the central IL-1 system via the β_2-adrenoceptor without provoking inflammatory response related behaviours in rats. *Brain Behav. Immun.* **56**, 114–129 (2016).
56. Frishman, W. Clinical pharmacology of the new β-adrenergic blocking drugs. Part 9. Nadolol: a new long-acting β-adrenoceptor blocking drug. *Am. Heart J.* **99**, 124–128 (1980).
57. Bilski, A. J., Halliday, S. E., Fitzgerald, J. D. & Wale, J. L. The pharmacology of a β_2-selective adrenoceptor antagonist (ICI 118,551). *J. Cardiovasc Pharm.* **5**, 430–437 (1983).
58. Jonsson, G., Hallman, H., Ponzio, F. & Ross, S. DSP4 (*N*-(2-chloroethyl)-*N*-ethyl-2-bromobenzylamine)—a useful denervation tool for central and peripheral noradrenaline neurons. *Eur. J. Pharm.* **72**, 173–188 (1981).
59. Farneback, G. Two-frame motion estimation based on polynomial expansion. *Proceedings of the 13th Scandinavian Conference on Image Analysis* 363–370 (2003).
60. Root, D. H. et al. Norepinephrine activates dopamine D4 receptors in the rat lateral habenula. *J. Neurosci.* **35**, 3460–3469 (2015).

nature research

Corresponding author(s): Dr. Ania Majewska

Last updated by author(s): 09/06/2019

Reporting Summary

Nature Research wishes to improve the reproducibility of the work that we publish. This form provides structure for consistency and transparency in reporting. For further information on Nature Research policies, see Authors & Referees and the Editorial Policy Checklist.

Statistics

For all statistical analyses, confirm that the following items are present in the figure legend, table legend, main text, or Methods section.

n/a	Confirmed	
☐	☒	The exact sample size (*n*) for each experimental group/condition, given as a discrete number and unit of measurement
☐	☒	A statement on whether measurements were taken from distinct samples or whether the same sample was measured repeatedly
☐	☒	The statistical test(s) used AND whether they are one- or two-sided *Only common tests should be described solely by name; describe more complex techniques in the Methods section.*
☐	☒	A description of all covariates tested
☐	☒	A description of any assumptions or corrections, such as tests of normality and adjustment for multiple comparisons
☐	☒	A full description of the statistical parameters including central tendency (e.g. means) or other basic estimates (e.g. regression coefficient) AND variation (e.g. standard deviation) or associated estimates of uncertainty (e.g. confidence intervals)
☐	☒	For null hypothesis testing, the test statistic (e.g. *F*, *t*, *r*) with confidence intervals, effect sizes, degrees of freedom and *P* value noted *Give P values as exact values whenever suitable.*
☒	☐	For Bayesian analysis, information on the choice of priors and Markov chain Monte Carlo settings
☒	☐	For hierarchical and complex designs, identification of the appropriate level for tests and full reporting of outcomes
☒	☐	Estimates of effect sizes (e.g. Cohen's *d*, Pearson's *r*), indicating how they were calculated

Our web collection on statistics for biologists contains articles on many of the points above.

Software and code

Policy information about availability of computer code

Data collection	Fluoview version 5 was used to collect all two-photon imaging data. A custom acquisition program written by Dr. Valery A. Kalatsky was used for intrinsic optical signal imaging, this program is: ContImage MFC Application Version 1.0.0.1. This program is commercially available from VKImaging. Prairie Ultima 4 was used for resonance image collection.
Data analysis	ImageJ 1.52n (FIJI) and associated plugins to the program were used to process two-photon imaging data for analysis. The Sholl analysis (v.4) plugin was used for morphological analysis. Matlab, 2018 version, was used for motility and laser ablation analysis. Custom scripts were written for these analyses and are available at https://github.com/majewska-lab. Prism version 6 was used for statistical analysis

For manuscripts utilizing custom algorithms or software that are central to the research but not yet described in published literature, software must be made available to editors/reviewers. We strongly encourage code deposition in a community repository (e.g. GitHub). See the Nature Research guidelines for submitting code & software for further information.

Data

Policy information about availability of data

All manuscripts must include a data availability statement. This statement should provide the following information, where applicable:

- Accession codes, unique identifiers, or web links for publicly available datasets
- A list of figures that have associated raw data
- A description of any restrictions on data availability

All data and code used for analysis will be made available when requested from the corresponding author, in addition the code for Matlab analysis is freely available at https://github.com/majewska-lab

Field-specific reporting

Please select the one below that is the best fit for your research. If you are not sure, read the appropriate sections before making your selection.

☒ Life sciences ☐ Behavioural & social sciences ☐ Ecological, evolutionary & environmental sciences

For a reference copy of the document with all sections, see nature.com/documents/nr-reporting-summary-flat.pdf

Life sciences study design

All studies must disclose on these points even when the disclosure is negative.

Sample size	No statistical methods were used to pre-determine sample sizes, but our sample sizes are similar to those reported in previous publications from our lab and other publications in the field. N's were also chosen such that we could determine if sex impacted our experimental results, thus sufficient males and females were included to meet this need. (Sipe, G. O., Lowery, R. L., Tremblay, M. È., Kelly, E. A., Lamantia, C. E., & Majewska, A. K. (2016). Microglial P2Y12 is necessary for synaptic plasticity in mouse visual cortex. Nature communications, 7, 10905.) as well as established n's from the literature.
Data exclusions	Exclusion data was pre-established as the following: animals with a compromised eye suture were excluded from the rest of IOS experiments, imaging sessions which were interrupted during the hour time course were terminated and that data was excluded from surveillance and motility due to the missing time points. Due to the nature of the laser ablation analysis the initial time point of the ablation was not part of the ablation analysis.
Replication	All attempts at replication of experiments were successful. Both in vivo two-photon imaging experiments and intrinsic optical signal imaging experiments were replicated and findings reproduced. Initially, pilot experiments with small cohorts were done for pharmacological manipulations of Beta2 signaling and anesthetic application which preceded our full cohort experiments. We also repeated effects seen in awake versus anesthetized mice across multiple control groups in our different sets of experiments. We see within our IOS data replication of our results across both BL6 mice and our Cx3cr1Cre control. For FACS sorting, multiple rounds of sorting and PCR were run to confirm excision of the Beta2 ARs. Histological experiments confirming DSP4 depletion were successful in small pilot experiments which preceded the full cohort of staining.
Randomization	Litters of mice were pseudo-randomized in assignment to experiments. It was not full randomization as there were efforts specifically made to distribute both males and females into our groups.
Blinding	Investigators were blinded to group allocation during all data analysis.

Reporting for specific materials, systems and methods

We require information from authors about some types of materials, experimental systems and methods used in many studies. Here, indicate whether each material, system or method listed is relevant to your study. If you are not sure if a list item applies to your research, read the appropriate section before selecting a response.

Materials & experimental systems

n/a	Involved in the study
☐	☒ Antibodies
☒	☐ Eukaryotic cell lines
☒	☐ Palaeontology
☐	☒ Animals and other organisms
☒	☐ Human research participants
☒	☐ Clinical data

Methods

n/a	Involved in the study
☒	☐ ChIP-seq
☐	☒ Flow cytometry
☒	☐ MRI-based neuroimaging

Antibodies

Antibodies used	BV786 rat anti-mouse CD11b (1:200, BD Pharmigen, 74086, clone: M1/70, lot#: 6168923). APC rat anti-mouse CD45 (1:400, BD Pharmigen, 561018, clone: 30-F11, lot#: 7163582). Iba1 rabbit anti-mouse (1:1000, Wako, 019-19741, lot#:019-19741). anti-tyrosine hydroxylase from mouse (1:400, has multiple mammalian reactivity, used for mouse labeling, Millipore, MAB318, clone: LNC1, lot# 3122928).
Validation	All of the utilized antibodies have either been validated in our lab with prior work or have validation information available on the manufacturer's website. All have citations in the literature confirming efficacy, and in our lab we have repeated experiments to confirm efficacy and dilution protocols. For the antibodies utilized in FACS experiments we have previously published utilizing these antibodies: Wong, E. L., Lutz, N. M., Hogan, V. A., Lamantia, C. E., McMurray, H. R., Myers, J. R., ... & Majewska, A. K. (2018). Developmental alcohol exposure impairs synaptic plasticity without overtly altering microglial function in mouse visual cortex. Brain, behavior, and immunity, 67, 257-278. For IBA-1 staining we have also previously published using this anti-body to label microglia and their processes for morphological analysis: Sipe, G. O., Lowery, R. L., Tremblay, M. È., Kelly, E. A., Lamantia, C.

E., & Majewska, A. K. (2016). Microglial P2Y12 is necessary for synaptic plasticity in mouse visual cortex. Nature communications, 7, 10905. For the tyrosine hydroxylase staining prior literature has confirmed the efficacy as detailed on the manufacturer's website: http://www.emdmillipore.com/US/en/product/Anti-Tyrosine-Hydroxylase-Antibody-clone-LNC1,MM_NF-MAB318#anchor_REF.

Animals and other organisms

Policy information about studies involving animals; ARRIVE guidelines recommended for reporting animal research

Laboratory animals	All strains of mice were on a C57/Bl6 background and between 3-17 weeks of age (P21-P120). CX3CR1-GFP(JAX: 005582) heterozygous mice were used to visualize microglia for in vivo two-photon imaging and were bred to THY1-YFP (JAX:003782) mice for spine contact imaging. CX3CR1-CreERT (JAX: 021160) mice were bred to Adrbeta2-flox3(Karsenty Lab courtesy of the Rosen Lab) mice to generate mice which had β2ARs selectively knocked out of microglia. CX3CR1-CreERT mice were also bred to Ai9 (tdTomato JAX: 007909). Males and Females were included in the study and the precise sex distribution by experiment is listed in Supplementary Table 1.
Wild animals	The study did not involve wild animals.
Field-collected samples	The study did not involve field-collected samples.
Ethics oversight	University of Rochester and Massachusetts Institute of Technology Committees on Animal Resources

Note that full information on the approval of the study protocol must also be provided in the manuscript.

Flow Cytometry

Plots

Confirm that:

☒ The axis labels state the marker and fluorochrome used (e.g. CD4-FITC).

☒ The axis scales are clearly visible. Include numbers along axes only for bottom left plot of group (a 'group' is an analysis of identical markers).

☒ All plots are contour plots with outliers or pseudocolor plots.

☒ A numerical value for number of cells or percentage (with statistics) is provided.

Methodology

Sample preparation	At ~P28 mice were euthanized by an i.p. sodium pentobarbital overdose (Euthasol, Virbac) and transcardially perfused with ice cold 0.15 M PBS. Each brain was removed and the whole cortex was dissected from the rest of the brain in ice cold, degassed FACS buffer (0.5% BSA, Sigma A2153 in 1x PBS Invitrogen 20012-027 pH 7.2). The tissue was kept on ice throughout all the procedures. Cortices were homogenized with a Dounce homogenizer and then passed through a 70µm filter and centrifuged (210xg, 7min, 4 °C). The supernatant was aspirated from the pellets and then the pellets resuspended and prepared for magnetic sorting with Myelin Removal Beads II (Miltenyi 130-0960733). The resuspended labelled tissue was passed through a 70µm filter and then the FACS buffer primed Magnetic columns (Miltenyi 130-096-733). After passage through the magnetic columns the samples were centrifuged, the supernatant removed, and resuspended in FACS buffer with Fc block (Biolegend 101320) for 15min at 4 °C. Samples were incubated with CD11b-AlexaFluor BV786 (BD Biosciences 740861) and CD45-APC (BD Biosciences 561018) for 30 min in the dark at 4°C. Each sort included the following compensation controls: BV720 bead control, APC bead control (eBiosciences 01-111-42), unstained live cells, and propidium iodide (PI) labelled Triton X-100 killed cells. An additional fully labelled sample was prepared with spare tissue to check the voltage settings prior to running experimental samples.
Instrument	18-color FACS Aria II flow cytometer
Software	FACS.Diva. version 8.0.1.
Cell population abundance	Cells were sorted for purity, and post-sort analysis in our lab have established that we get 98.8 +/- 0.78% accuracy with 83.0 +/- 2.8% cell viability. For our experiments in supplemental figure 8our cell yield in mice not dosed with tamoxifen was 18K, 74.5K, and 50K. For mice dosed with tamoxifen 34K, 25K, and 23K.
Gating strategy	The same gating strategy was applied across all the sorts and is represented with our sample sort in Supplemental Figure 15.

☒ Tick this box to confirm that a figure exemplifying the gating strategy is provided in the Supplementary Information.